7-30-1996

Characterization and modeling of multi-conductor transmission line using Finite-difference Time-Domain method

Sanjay Bajracharya
Florida International University

DOI: 10.25148/etd.FI14050409

Florida International University
Miami, Florida

Characterization and modeling of Multi-Conductor Transmission Line using Finite-Difference Time-Domain method

A thesis submitted in partial satisfaction of the requirements for the degree of
MASTER OF SCIENCE
in
ELECTRICAL ENGINEERING

by

Sanjay Bajracharya

1996

To: Dean Gordon R. Hopkins
College of Engineering and Design

This thesis, written by Sanjay Bajracharya, and entitled, Characterization and modeling of Multi-Conductor Transmission Line using Finite-Difference Time-Domain method, having been approved in respect to style and intellectual content, is referred to you for judgment.

We have read this thesis and recommend that it be approved.

Gustavo Roig

Malcolm Heimer

Tadeusz M. Babij/James R. Story
Major Professor

Date of Defense: July 30, 1996

This thesis of Sanjay Bajracharya is approved.

Dean Gordon R. Hopkins
College of Engineering
and Design

Dr. Richard L. Campbell
Dean of Graduate Studies

Florida International University, 1996

I dedicate this thesis to my wife and my parents.

Without their patience, understanding, support, and most of all love,

the completion of this work would not have been possible.

ACKNOWLEDGMENTS

I wish to thank Dr. Tadeusz M. Babij, my major professor, for his valuable help during the whole course of this thesis work. I also thank Dr. Gustavo Roig and Dr. Malcolm Heimer for their helpful comments and patience when reviewing this thesis. This project is supported by the Department of the Army, Grant DAAH04-93-6-0482, the National Science Foundation, Grant CDA9313624 and the U.S. Air Force, Office of Scientific Research, Grant F49620-95-1-0519.

I take this opportunity to express my deep gratitude to my friends Carl C. Chen and Shengyao Hu for their great help with suggestions and corrections on writing this paper, as well as Richard Millard and Arnaldo J. Sans for their beneficial discussion about this project. I would also like to thank Noemi Fernandez for all the help with the SGI-Indy work stations.

Finally, I thank my wife, Shailina Bajracharya and my parents for their patience and dedication through all the months of work.

ABSTRACT OF THE THESIS

Characterization and modeling of Multi-Conductor Transmission Line using Finite-Difference Time-Domain method

by

Sanjay Bajracharya

Florida International University, 1996

Miami, Florida

Tadeusz M. Babij, Major Professor

A two-dimensional, 2D, finite-difference time-domain (FDTD) method is used to analyze two different models of multi-conductor transmission lines (MTL). The first model is a two-conductor MTL and the second is a three-conductor MTL. Apart from the MTL's, a three-dimensional, 3D, FDTD method is used to analyze a three-patch microstrip parasitic array. While the MTL analysis is entirely in time-domain, the microstrip parasitic array is a study of scattering parameter S_{11} in the frequency-domain. The results clearly indicate that FDTD is an efficient and accurate tool to model and analyze multiconductor transmission line as well as microstrip antennas and arrays.

Table of Contents

CHAPTER PAGE

Acknowledgements ..... **iv**

Abstract ..... **v**

Table of Contents ..... **vi**

List of Figures ..... **viii**

1. Introduction **1**

1.1 Scope of this Thesis 1

1.2 Resource Requirements 3

1.3 Excitation Pulse Used 3

2. Finite-Difference Time-Domain (FDTD) Method **7**

2.1 Principals of FDTD Method 9

2.2 Absorbing Boundary Condition 13

2.3 Other Methods for Electromagnetic Computation 17

3. The Multi-Conductor Transmission Line **18**

3.1 Derivation from the Integral Form of Maxwell's Equations 19

3.2 Derivation from the Per-Unit-Length Equivalent Circuit 27

3.3 Summary of the MTL Equations 29

4. Time-Domain Analysis **32**

4.1 **Case I**, Two-Conductor MTL 32

4.1.1 Computed Results 33

4.1.2 Validation 37

4.1.2.1 Analytical Simulation 38

4.1.2.2 SPICE Simulation 38

4.2 **Case II,** Three-Conductor MTL 49

4.2.1 Computed Results 49

4.2.2 Validation 53

4.2.2.1 SPICE Simulation 53

5. Frequency-Domain Analysis 60

5.1 Fourier Transform 60

5.2 **Case III,** Microstrip Parasitic Array 62

5.3 Computed Results 64

5.4 Validation 67

6. Conclusion and Future Works 72

Conclusion 72

Future Works 75

References 76

Appendix 80

List of Figures

Fig. 1.1 Trapezoidal pulse 4

Fig. 1.2 Gaussian Pulse 5

Fig. 1.3 Fourier transform of Gaussian Pulse 6

Fig. 2.1 Yee Cell 8

Fig. 2.2 Mur's Absorbing Boundary Condition (ABC) 14

Fig. 3.1 Definition of the contour for derivation of MTL equation 22

Fig. 3.2 Definition of the surface for derivation of MTL equation 24

Fig. 3.3 Per-Unit-Length MTL model 28

Fig. 4.1 Electrical schematic of two-conductor MTL 33

Fig. 4.2 End-on view of structure of two-conductor MTL 36

Fig. 4.3 Near-End Voltage of two-conductor MTL (FDTD method) 39

Fig. 4.4 Far-End Voltage of two-conductor MTL (FDTD method) 40

Fig. 4.5 Near-end Voltage of two-conductor MTL (Analytical method) 41

Fig. 4.6 Far-end Voltage of two-conductor MTL (Analytical method) 42

Fig. 4.7 Near-end Voltage of two-conductor MTL (SPICE method) 43

Fig. 4.8 Far-end Voltage of two-conductor MTL (SPICE method) 44

Fig. 4.9 Near-end Voltage of two-conductor MTL combined 45

Fig. 4.10 Far-end Voltage of two-conductor MTL combined 46

Fig. 4.11 Near-end Voltage of two-conductor MTL (subplots) 47

Fig. 4.12 Far-end Voltage of two-conductor MTL (subplots) 48

Fig. 4.13 End-on view of structure of three-conductor MTL 50

Fig. 4.14 Electrical schematic of three-conductor MTL 51

Fig. 4.15 Representation of three-conductor MTL 54

Fig. 4.16a Near-end Voltage of three-conductor MTL (FDTD and SPICE) 57

Fig. 4.16b Near-end Voltage of three-conductor MTL (FDTD and SPICE) 58

Fig. 4.16c Near-end Voltage of three-conductor MTL (FDTD and SPICE) 59

Fig. 5.1 Three-patch coplanar parasitic array structure 63

Fig. 5.2 3D structure of three-patch coplanar parasitic array structure 64

Fig. 5.3 Comparison study of center frequency 67

Fig. 5.4 Comparison study of drop in S_{11} 68

Fig. 5.5 Set I - S_{11} parameter for a three-patch parasitic array 70

Fig. 5.6 Set II - S_{11} parameter for a three-patch parasitic array 71

Chapter 1

Introduction

1. INTRODUCTION

Of the four forces in nature - strong, weak, electromagnetic, and gravitational - the electromagnetic force is the most technologically pervasive. Of the three methods of predicting electromagnetic effects - experiment, analysis and computation, computation is the newest and fastest growing approach. Of all the methods used for electromagnetic computation (discussed in Chapter 2.3), the finite-difference time-domain, FDTD, method is applicable to the widest range of problems [3].

1.1 SCOPE OF THIS THESIS

The goal of this thesis is to develop an efficient technique by using FDTD method to help analyze and design multi-conductor transmission line (MTL) and microstrip parasitic array. Many works have been done since the introduction of FDTD method. Discrete modeling of space and time, improved first-order and second-order absorbing boundary conditions, increase in speed of computation

by better computer, faster algorithm and parallel computing are a few examples of improvement for better and accurate electromagnetic computation.

Zhang *et al* (1987), used the FDTD method to investigate microstrip discontinuity problems [17]. Zhang *et al* (1987) [17], Sheen *et al* (1990) [12] and Lee *et al* (1994) [15] further applied FDTD method to analyze microstrip patch antennas and other microstrip circuits. In this thesis, three different models are analyzed. The first two models are a two-conductor and a three-conductor multi-conductor transmission lines. Both the cases are analysis in the time-domain, using two-dimensional FDTD algorithm. Case I (Chapter 4.1), a two-conductor MTL, is based on Kraus [8]. The result is compared with analytical results based on BASIC program [8] and SPICE simulation. This is a simple two-conductor MTL with a source resistance and a load resistance. Computed results are very much in agreement with each other. Case II (Chapter 4.2) is a three-conductor MTL based on Marx *et al* [5]. Of the three conductors in the MTL, one conductor has a source resistance, an excitation pulse and a load resistance. The second conductor has a near-end resistance and a far-end resistance. The third and final conductor is taken as the reference conductor for return path. Marx *et al* used the model with simulation in SPICE program. Anyhow, in this thesis, FDTD algorithm is applied and the results are compared with the SPICE result of Marx *et al* [5]. Here also, there is good agreement between the FDTD and the SPICE result. Case III (Chapter 5.1) is a three-patch coplanar parasitic array, where

three-dimensional FDTD analysis is conducted and the results are studied in frequency-domain. The scattering parameter S_{11} is compared with experimental results [15] and the results of Lee *et al* [15].

1.2 RESOURCE REQUIREMENTS

Both the FDTD codes, two-dimensional and three-dimensional, are written in FORTRAN. Computer simulation for the MTL models, two-dimensional FDTD code are done in SOLIX, the university's computing system. Anyhow, for the three-dimensional FDTD code, as a bigger and better computing environment is needed, a SUN SPARC Station 10 is used. Some of the computations are also done in the SGI-Indy work stations in the Center for Advanced Technology and Education (CATE) Lab. All of the graphical analysis are done using MATLAB, either on a PC or the SERVMS system.

1.3 EXCITATION PULSE USED

The excitation pulse or the incident field for the simulations are different based on the models used. Basically, two types of excitation pulses are used. For case I and II, both MTL models, a trapezoidal pulse is used, while for case III, a Gaussian pulse is used. For a trapezoidal pulse, the width of the pulse is kept

small in comparison to the final solution time. A typical trapezoidal pulse [6] is shown in Fig. 1.1.

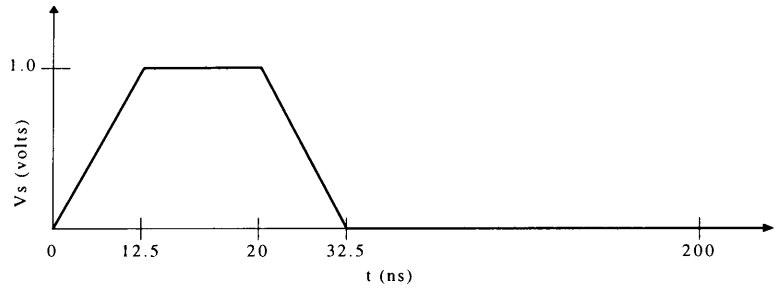

Fig. 1.1 Trapezoidal pulse used as incident source in MTL models

Here the rise and fall time is 12.5 ns and the pulse width is 7.5 ns (20 ns at an average). The final solution time is 200 ns. To define this trapezoidal pulse in SPICE simulation, following command is used [11].

```
PULSE(0 1 0 12.5N 12.5N 7.5N 200N)
```
(1.1)

A Gaussian pulse is given by the expression

$$g = \exp\left[-\frac{(t-t_0)^2}{T^2}\right] \tag{1.2}$$

where t_0 is the time shift and T is the width of the pulse. In general, t_0 is taken as $3 \times T$. A Gaussian pulse has a smooth waveform in time, as shown in Fig. 1.2 for a pulse width T of 50 ps and t_0 of 150 ps ($3 \times T$). It's Fourier transform (spectrum) is also a Gaussian pulse centered at zero frequency. These unique properties make it a perfect choice for investigating the frequency-dependent characteristics of the microstrip array via the Fourier transform of the pulse

response [17]. The Fourier transform, FFT, of the Gaussian source is shown in Fig. 1.3. The Gaussian pulse is then truncated at around 300 ps, after the pulse has been fully launched [3].

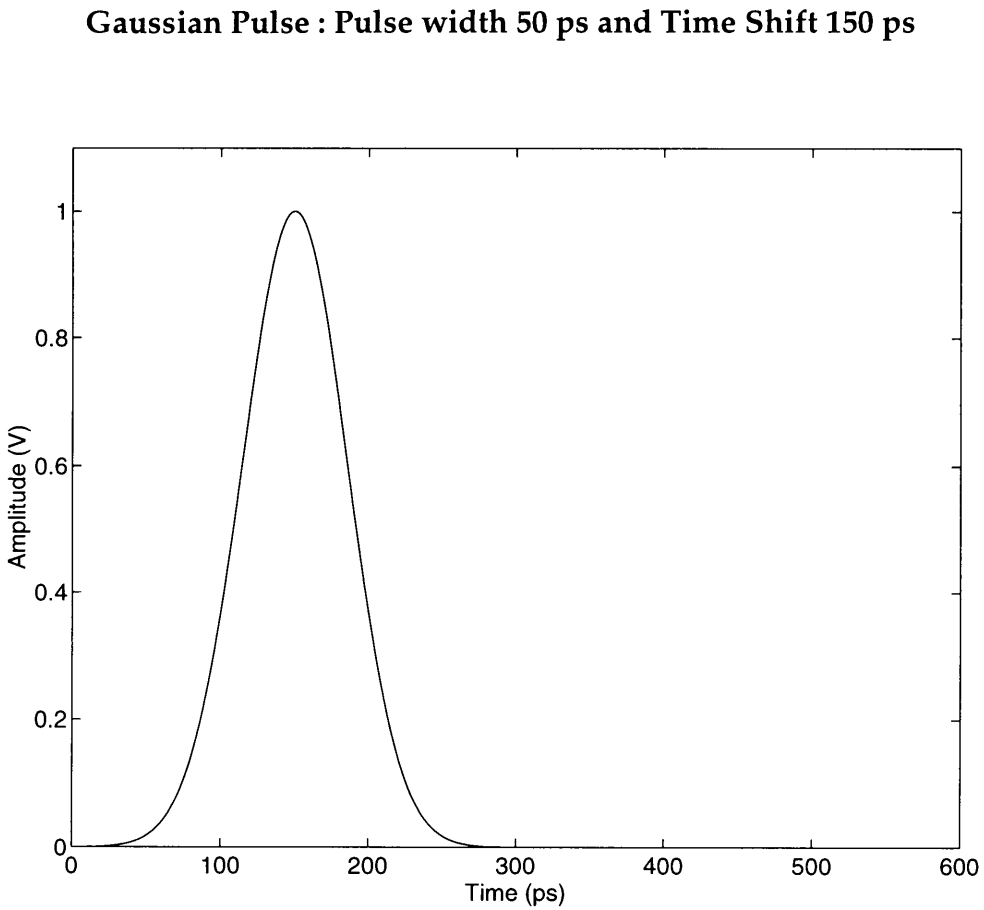

Fig. 1.2 Gaussian pulse based on (1.2) with a pulse width of 50 ps [3].

Fourier transform of Gaussian Pulse : Pulse width 50 ps and Time Shift 150 ps

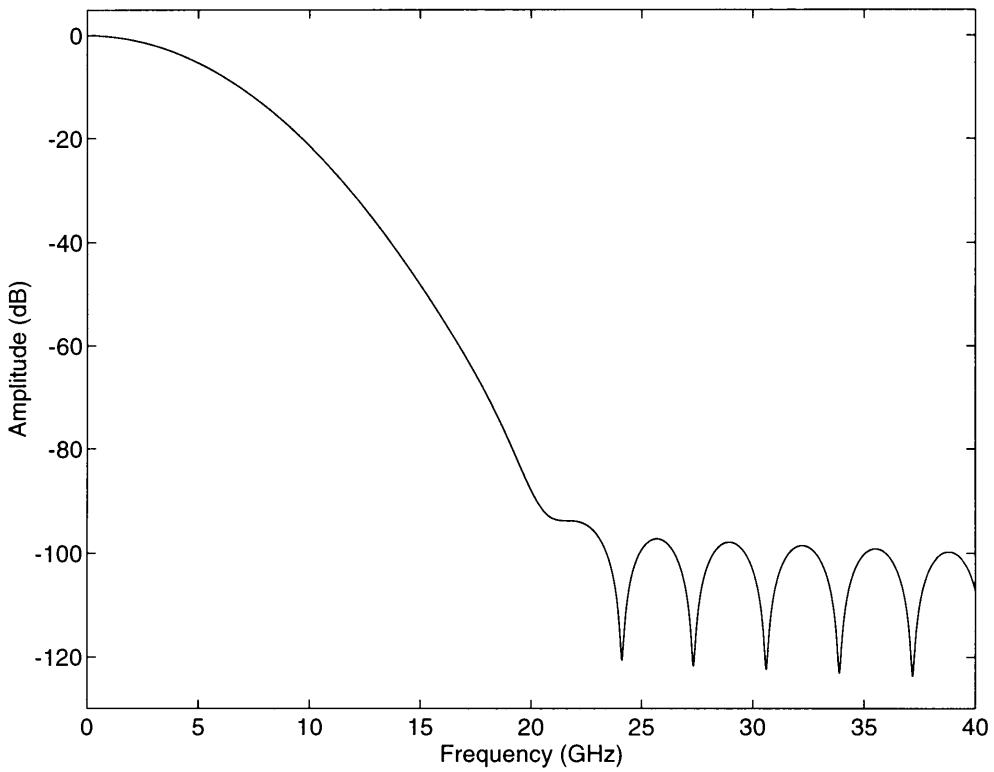

Fig. 1.3 Fourier transform of the Gaussian pulse of Fig. 1.2.

Chapter 2

Finite-Difference Time-Domain Method

2. FDTD METHOD

The Finite-Difference Time-Domain, FDTD, algorithm was first introduced by Kang S. Yee in 1966 [1]. Although the FDTD method has existed for 30 years, it has received more attention in the recent years. Furthermore, extensions and enhancements to the method are continually being published, which further broaden it's appeal. Earlier applications of FDTD were mainly in the electromagnetic scattering, but recently a number of researchers have applied the FDTD method to analyze antenna problems also. This algorithm can be used to analyze antenna of any shape, including thick substrates with fringing field effects. In addition , feed networks and arrays of elements may also be modeled. Antennas that have been analyzed by the FDTD method include planar and stacked microstrip antennas with probe or aperture-coupled feeds. Results from these analysis, such as input impedance and reflection coefficients, and specially the scattering parameter S_{11}, have shown good agreement with experiments [15].

Yee Cell Cube

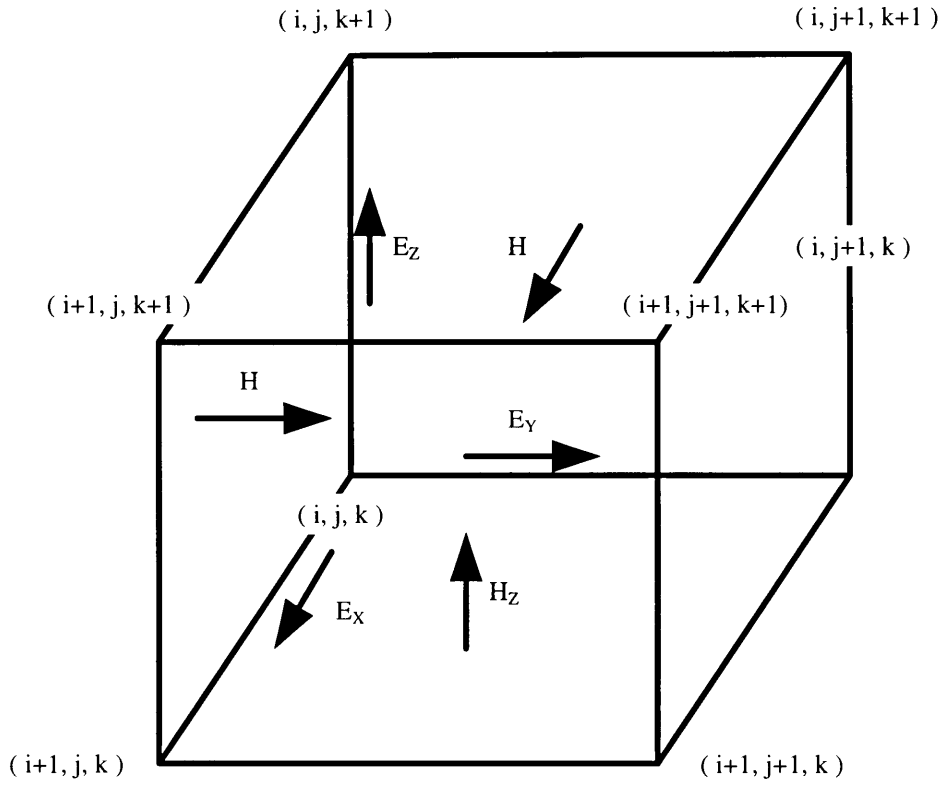

Fig 2.1. The Yee cell (i, j, k) with the six (i, j, k) field components shown. The remaining edges and faces also have fields that are labeled as belonging to neighboring cells [3].

The FDTD method for solving electromagnetic scattering problems is based on the finite-difference discretization of Maxwell's equations in both space and time-domain.

The FDTD cube, as originally described by Yee, is shown in Fig. 2.1. This method is second-order accurate on account of the central differencing scheme used in approximating the differentials. Second-order accurate means that the first-order error terms of the equations vanish leaving only second and higher order error terms in time and space [14].

2.1 PRINCIPALS OF FDTD METHOD

In a linear medium, the differential time-domain Maxwell's equations are

$$\nabla \times E = -\frac{\partial B}{\partial t} \tag{2.1}$$

$$\nabla \times H = \frac{\partial D}{\partial t} + J \tag{2.2}$$

$$\nabla . D = \rho \tag{2.3}$$

$$\nabla . B = 0 \tag{2.4}$$

This is all the information needed for linear isotropic materials to completely specify the field behavior over time, so long as the initial field distribution is specified and satisfies the Maxwell equations. Conveniently, the field and source are set to zero at the initial time, often taken as time zero.

The starting point for the FDTD formulation is the curl equations. They can be reset to the form used for FDTD

$$\frac{\partial H}{\partial t} = -\frac{1}{\mu}(\nabla \times E) - \frac{\sigma^*}{\mu} H \tag{2.5}$$

$$\frac{\partial E}{\partial t} = \frac{-\sigma}{\varepsilon} E + \frac{1}{\varepsilon}(\nabla \times H) \tag{2.6}$$

where $J = \sigma E$ to allow for lossy dielectric material and have included the possibility of magnetic loss by adding a magnetic conductivity term σ^* [3] .

In the FDTD method, the workspace is divided into cells. Each cell has a corresponding material type, which is specified in terms of cell's permittivity, ε, and permeability, μ, for dielectric materials. A material may also be defined as a perfect electrical conductor (PEC), in which case, the total fields in that cell are set equal to zero. In each cell, the six electromagnetic fields, E_X, E_Y, E_Z, H_X, H_Y, and H_Z are defined at specific locations. Equations (2.5) and (2.6) are discretized in both time and space using the central finite difference method (2.7) and solved at all points inside the workspace. With the central finite difference method, the equations are linear and no matrix needs to be solved or inverted. At time $t = 0$, all fields are set equal to zero. As the time is incremented, a source is inserted into the workspace. For scattering problems, the source is usually a plane wave that is allowed to propagate into the workspace. For radiation problems, the

source usually occupies a fixed location in the workspace and is gradually ramped up in amplitude.

$$f'(x) \approx \frac{f(x_0 + \Delta x) - f(x_0 - \Delta x)}{2\Delta x} \tag{2.7}$$

The direct output of FDTD is information regarding the time-domain response of the model. This includes, determining the electromagnetic fields over space at a specific time, as well as the fields at a specific location as a function of time. Two types of sources are of primary interest in transmission line design. If a finite pulse (such as Gaussian pulse) is excited, then time is advanced until the pulse propagates through the workspace and the fields in the workspace have died down to zero. Then Fourier transform is used to transform to the frequency-domain for computing input transmission line parameters. If a single frequency sinusoid is used as the source, then time is advanced until the fields reach steady state. At this time, the near-fields can be sampled. Two types of far fields information may be obtained. If a pulse is used, then a far field transformation can be used to determine the far field at a given observation point for a wide range of frequencies. If a single frequency sinusoid is used, then the far field pattern for many observation angles can be calculated at a single frequency [15].

The first step in designing a model with FDTD code is to grid up the object. A number of parameters must be considered in order for the code to work successfully. The grid spacing must be small enough so that the fields are

sampled sufficiently to ensure accuracy [15]. In the conventional algorithm, a uniform spatial grid is employed. To obtain good accuracy using this method, the smallest discretization Δz is chosen to be on the order of $\frac{\lambda_{hf}}{10}$ to $\frac{\lambda_{hf}}{20}$, where λ_{hf} is the minimum wavelength in the structure at the highest frequency of interest [14]. This is roughly the same grid density needed for Method of Moment (MoM), but FDTD scales upwards in frequency better than MoM [15].

Once the spatial discretization Δz is chosen, the time step Δt is chosen such that numerical instabilities are avoided, according to the Courant stability condition [15], given by

$$\Delta t \leq \frac{1}{c} \frac{1}{\sqrt{\frac{1}{(\Delta x)^2} + \frac{1}{(\Delta y)^2} + \frac{1}{(\Delta z)^2}}} \tag{2.8}$$

where c is the maximum velocity of propagation in any medium, Δx, Δy and Δz are the grid size chosen in the x, y and z directions respectively. This condition prevents a signal from crossing a cell in less than about a time step, ensuring that information does not skip across a cell [15]. To speed up computation, it is advantageous to use large temporal discretization. Given the grid size, the size of the workspace (in cells) can be determined. The workspace must be large enough not only to include the object, but also a buffer zone around it. Since most absorbing boundary conditions (ABC) are only approximate, there will be reflections from the walls of the workspace, particularly when the boundary wall

is inhomogeneous (e.g., the dielectric substrate goes up to the side wall of the workspace) [15].

2.2 ABSORBING BOUNDARY CONDITION

Another important issue of FDTD algorithm is the formulation of absorbing boundary condition, ABC, or outer radiation boundary condition. This condition is needed only when the object is in the infinite free space. Formulating a problem space large enough that the waves never reach the boundary requires tremendous memory leading to computational cost and thus almost impossible. The goal of the ABC is to mathematically simulate the infinite free space so that the waves continuously propagate without reflection. If an ABC on the boundaries of the problem space is not formulated appropriately, FDTD fields calculating formulas are not able to use the correct values to update the fields. That is, the fields are reflected on the boundaries instead of propagating outward continuously. This is due to the nature of the FDTD formulas, they use the field values of the adjacent cells to interpolate the fields values of the current cell.

The perfect ABC is usually global in nature, which makes it quite expensive to implement and require excessive large computer memories. The local ABC, which make use of only the neighboring space and time nodes, are

relatively inexpensive to implement. There are quite a few local ABC's available. The Fourier transform of the time-domain results are very sensitive to the reflection errors. A small amount of reflection may not visibly influence the time-domain fields, but the transformed results could be far off [17]. Zhang *et al.* [17] employed a super-position of two subproblems with magnetic and electric walls to cancel the boundary reflection.

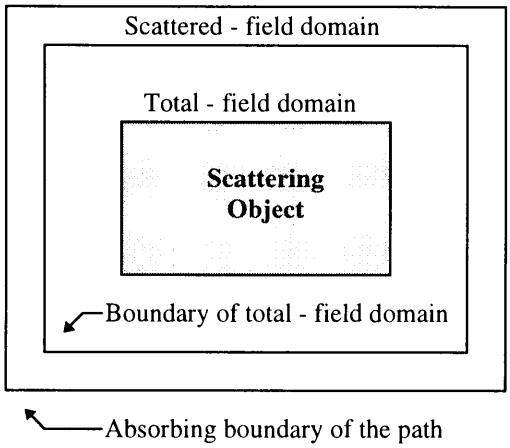

Fig. 2.2 The domain occupied by the mesh with the obstacle, the domain where the total field is computed, and the domain where the scattered field is computed (two-dimensional configuration) [2].

ABC scheme has been developed from as early as 1975 by Taflove to the present days. But the most popular and widely used among all of them is the one

put forward by Mur in 1981 [2]. In this thesis work, only the first-order Mur absorbing formulas, which use the previous time-step and space grid to simulate the infinite space, is utilized because they provide acceptable accuracy. Higher order absorbing formulas will further improve the accuracy but require much adaptation to be applied in microstrip structures [12] [18].

Recently more accurate ABC's have been proposed, such as super absorption and perfectly matched layer (PML). Although these advancements in ABC significantly decrease the residual in the time-domain, they are more complicated in implementation than the simple ABC's such as Mur's [2]. Second, the FDTD method is quiet memory intensive since the core memory is directly proportional to the number of cells used in the discretization of the computational volume. The computational volume can be reduced by using a low reflection ABC such as Berenger's PML, which allows close proximity between the boundary wall and the circuit away from discontinuities. It is possible to reduce the computational domain even for the simple Mur's ABC, *if the boundary reflection can be accurately estimated and applied to correct the computed parameters* [19]. The concept of Mur's ABC is illustrated in Fig. 2.2 [2].

The first order ABC formulas require the physical problem space boundary to be set to 10 cells or more away from the object so that the fields can be absorbed normally. Higher order ABC formulas need less cells to get the same level of accuracy.

In Mur's ABC, the first order three-dimensional scalar wave equation is

$$(\partial_x^2 + \partial_y^2 + \partial_z^2 - c_0^{-2}\partial_t^2)E = 0 \tag{2.9}$$

where E is any field component, c_0 is the speed of light in free space. The FDTD theory can be used to discretize E_Z from the above equation which yields

$$\begin{aligned} E_z^{n+1}(0, j, k+\frac{1}{2}) &= E_z^n(1, j, k+\frac{1}{2}) \\ &+ \frac{c_0\delta t - \delta}{c_0\delta t + \delta}(E_z^{n+1}(1, j, k+\frac{1}{2}) \\ &- E_z^n(0, j, k+\frac{1}{2})). \end{aligned} \tag{2.10}$$

The other two ABC formulas for E_X and E_Y can be easily derived by the same procedure as given below

$$\begin{aligned} E_x^{n+1}(i+\frac{1}{2}, 0, k) &= E_x^n(i+\frac{1}{2}, 1, k) \\ &+ \frac{c_0\delta t - \delta}{c_0\delta t + \delta}(E_x^{n+1}(i+\frac{1}{2}, 1, k) \\ &- E_x^n(i+\frac{1}{2}, 0, k)). \end{aligned} \tag{2.11}$$

and

$$\begin{aligned} E_y^{n+1}(i, j+\frac{1}{2}, 0) &= E_y^n(i, j+\frac{1}{2}, 1) \\ &+ \frac{c_0\delta t - \delta}{c_0\delta t + \delta}(E_y^{n+1}(i, j+\frac{1}{2}, 1) \\ &- E_y^n(i, j+\frac{1}{2}, 0)). \end{aligned} \tag{2.12}$$

2.3 OTHER METHODS FOR ELECTROMAGNETIC COMPUTATION

Various methods used for electromagnetic computation are method of moments (MoM), finite-difference time-domain method (FDTD), finite element, geometric theory of diffraction, physical optics [15] and Bergeron's Method [17]. This thesis work focuses entirely on FDTD method.

The advantage of FDTD method over other method is that any antenna model, MTL model or microstrip antenna can be simulated easily. The only disadvantage is, as the model object increases, bigger work space is needed, which is computer costly. FDTD method can accurately simulate in high frequency range, which cannot be achieved from MoM method.

Chapter 3

The Multi-Conductor Transmission Line

3. THE MULTI-CONDUCTOR TRANSMISSION LINE

The term multi-conductor transmission line (MTL) equation typically refers to a set of (n+1) parallel conductors that serve to transmit electrical signals between sources and loads. The dominant mode of propagation in an MTL is the transverse electromagnetic or TEM mode, where, the electric and magnetic fields surrounding the conductors lie solely in the transverse plane, orthogonal to the line axis. The TEM field structure and associated mode of propagation is the fundamental, underlying assumption in the representation of a transmission line structure with the transmission line equations. The signal propagation is restricted to situations in which the propagation velocity on the line is unique. The conductors of the transmission lines are either lossy or lossless. Lossless conductors are perfect conductors, while lossless media have zero conductivity (σ = 0). The surrounding medium may be *homogeneous* or *inhomogeneous.* The FDTD model used in the examples are, by implication, immersed in a homogeneous medium (logically free space) [6].

3.1 DERIVATION FROM THE INTEGRAL FORM OF MAXWELL'S EQUATIONS

Figure 3.1 shows the general (n+1)-conductor line to be considered. It consists of n conductors and a *reference conductor* (denoted by zeroth conductor) to which the n line voltages will be referenced. This choice of reference conductor is not unique. From Faraday's law in integral form we have

$$\oint_C \vec{\mathrm{E}} \cdot d\vec{l} = -\mu \frac{d}{dt} \int_s \vec{\mathrm{H}} \cdot \vec{ds} \tag{3.1}$$

Applying this to the contour c_i which encloses surface s_i shown between the reference conductor and the i-th conductor and encircles it in the clockwise direction gives

$$\int_a^{a'} \vec{\mathrm{E}}_t \cdot d\vec{l} + \int_{a'}^{b'} \vec{\mathrm{E}}_l \cdot d\vec{l} + \int_{b'}^{b} \vec{\mathrm{E}}_t \cdot d\vec{l} + \int_b^a \vec{\mathrm{E}}_l \cdot d\vec{l} = \mu \frac{d}{dt} \int_{s_i} \vec{\mathrm{H}}_t \cdot \vec{a}_n ds \tag{3.2}$$

where $\vec{\mathrm{E}}_t$ denotes the transverse electric field (in the x-y cross-sectional plane) and $\vec{\mathrm{E}}_l$ denotes the *longitudinal* or *z-directed* electric field (along the surface of the conductor). Because of the choice of the direction of the contour, the direction $\vec{a}_n$, and the right-hand rule, the minus sign on the right hand side of the Faraday's law is absent (3.2). Because of the assumption of a TEM field structure, one can *uniquely* define voltage between the i-th conductor and the reference conductor (positive on the i-th conductor) as

$$V_i(z,t) = -\int_a^{a'} \vec{\mathrm{E}}_t(x,y,z,t) \cdot d\vec{l} \tag{3.3a}$$

$$V_i(z+\Delta z,t) = -\int_b^{b'} \vec{\mathrm{E}}_t(x,y,z+\Delta z,t)\cdot d\vec{l} \tag{3.3b}$$

The integrals along the surface of the conductors are zero if the conductors are considered to be perfect conductors. The TEM mode cannot exist if the conductors are not perfect conductors. This is because a component of electric field will be directed in the z direction due to the voltage drop along the conductors. The current is *uniquely defined* because of the assumption of a TEM field structure, as

$$I_i(z,t) = \oint_{\hat{c}i} \vec{\mathrm{H}}_t \cdot d\vec{l} \tag{3.4}$$

and contour $\hat{c}_i$ is a contour just off the surface of and encircling the i-th conductor in the transverse plane. The sum of the currents on all (n +1) conductors in the z direction at any cross section is zero. This is the basis for saying that the currents of the n conductors return through the *reference conductor*. Substituting (3.3) to (3.4) into (3.2) yields

$$-V_i(z,t) + r_i\Delta z I_i(z,t) + V_i(z+\Delta z,t) + r_0\Delta z\sum_{k=1}^{n} I_k(z,t) = \mu\frac{d}{dt}\int_{s_i} \vec{\mathrm{H}}_t\cdot\vec{a}_n ds \tag{3.5}$$

Dividing both sides by Δz, and rearranging gives

$$\begin{aligned}\frac{V_i(z+\Delta z,t)-V_i(z,t)}{\Delta z} &= -r_0 I_1 - r_0 I_2 - \ldots\ldots - (r_0+r_i)I_i - \ldots . r_0 I_n \\ &\quad + \mu\frac{1}{\Delta z}\frac{d}{dt}\int_{s_i} \vec{\mathrm{H}}_t\cdot\vec{a}_n ds\end{aligned} \tag{3.6}$$

The total magnetic flux penetrating the surface s_i can be written as

$$\psi_i = -\mu \lim_{\Delta z \to 0} \frac{1}{\Delta z} \int_{s_i} \vec{H}_t \cdot \vec{a}_n ds$$
$$l_{i1} I_1 + l_{i2} I_2 + ... + l_{ii} I_i + ... + l_{in} I_n \tag{3.7}$$

Taking the limit of (3.6) as $\Delta z \to 0$, and substituting (3.7) yields

$$\frac{\partial V_i z,t)}{\partial} = -r_0 I_1(z,t) - r_0 I_2(z,t) - ..... - (r_0 + r_i) I_i(z,t) - .... - r_0 I_n(z,t)$$
$$- l_{i1} \frac{\partial I_1(z,t)}{\partial} - l_{i2} \frac{\partial I_2(z,t)}{\partial} - .... - l_{ii} \frac{\partial I_i(z,t)}{\partial} - .... - l_{in} \frac{\partial I_n(z,t)}{\partial} \tag{3.8}$$

This first MTL equation can be written in compact form using matrix notation as

$$\frac{\partial}{\partial z} V(z,t) = -RI(z,t) - L \frac{\partial}{\partial t} I(z,t) \tag{3.9}$$

where the voltage and current vectors are defined as

$$V(z,t) = \begin{bmatrix} V_1(z,t) \\ V_i(z,t) \\ \vdots \\ V_n(z,t) \end{bmatrix} \tag{3.10a}$$

$$I(z,t) = \begin{bmatrix} I_1(z,t) \\ I_i(z,t) \\ \vdots \\ I_n(z,t) \end{bmatrix} \tag{3.10b}$$

The *per-unit-length inductance matrix* is defined from (3.7) as

$$\Psi = LI \tag{3.11}$$

where ψ is an $n \times 1$ vector containing the total magnetic flux per unit length, ψ_i, penetrating the i-th conductor and the reference conductor. The *per-unit-length inductance matrix*, L, contains the individual per-unit-length self-inductance's, l_{ii}, of the circuit and the per-unit-length mutual inductance between the circuits, l_{ij},

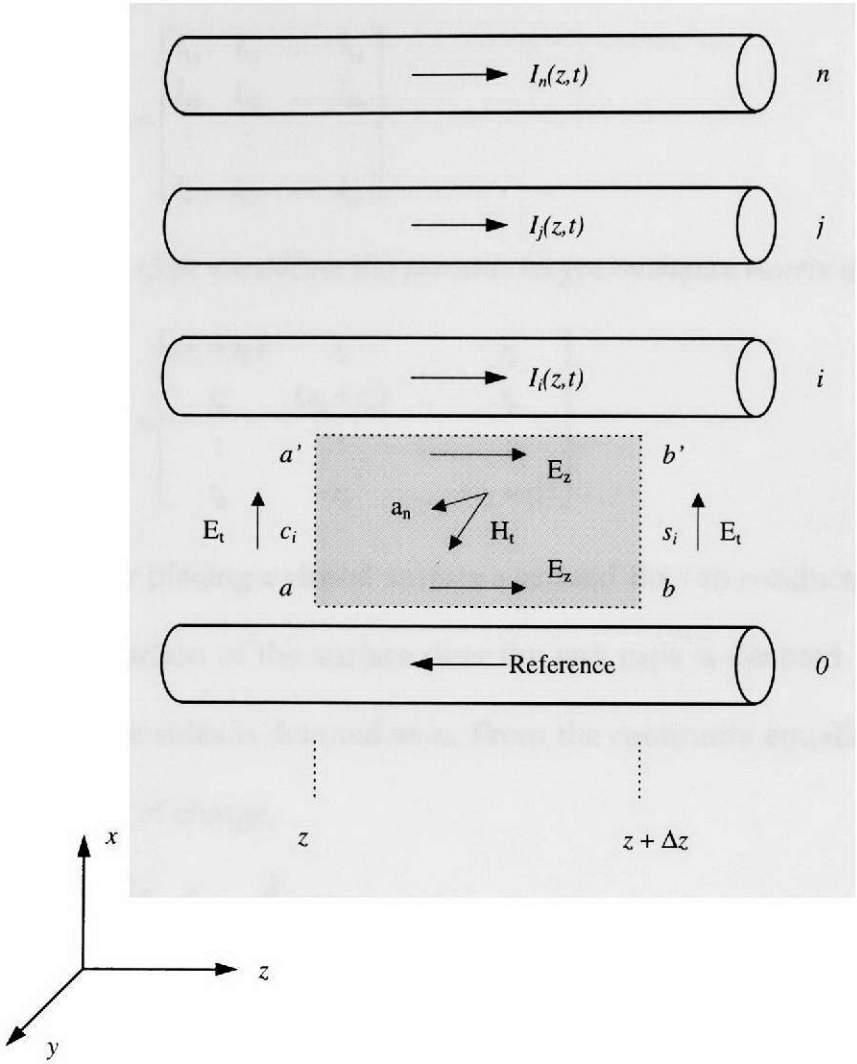

Fig 3.1 Definition of the contour for derivation of the MTL equation [6].

as

$$L=\begin{bmatrix} l_{11} & l_{12} & .. & l_{1n} \\ l_{21} & l_{22} & .. & l_{2n} \\ : & : & :: & : \\ l_{n1} & l_{n2} & .. & l_{nn} \end{bmatrix} \tag{3.12}$$

Similarly, from (3.8) we define the *per-unit-length resistance matrix* as

$$R=\begin{bmatrix} (r_1+r_0) & r_0 & .. & r_0 \\ r_0 & (r_2+r_0) & .. & r_0 \\ : & : & :: & : \\ r_0 & r_0 & .. & (r_n+r_0) \end{bmatrix} \tag{3.13}$$

Consider placing a closed surface s around the i-th conductor as shown in Fig. 3.2. The portion of the surface over the end caps is denoted as s_e while the portion over the sides is denoted as s_0. From the continuity equation or equation of conservation of charge,

$$\oiint_{\bar{s}} \vec{\vartheta} \cdot d\vec{s} = -\frac{\partial}{\partial t} Q_{\text{enc}} \tag{3.14}$$

Over the end caps we have

$$\iint_{\bar{S}_e} \vec{\vartheta} \cdot d\vec{s} = I_i(z+\Delta z,t) - I_i(z,t) \tag{3.15}$$

Over the sides of the surface, there are two currents : *conduction current,* and *displacement current,* where the surrounding homogeneous medium is characterized by conductivity, σ, and permittivity, ε.

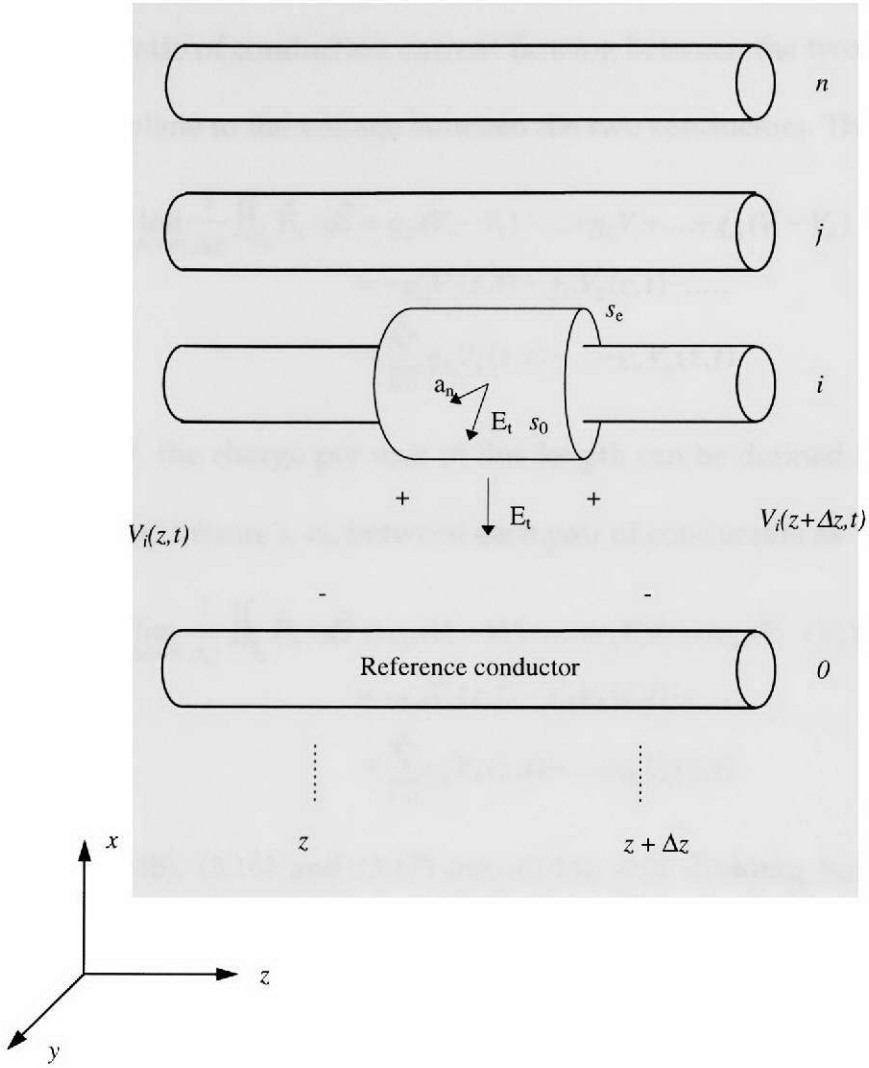

Fig 3.2 Definition of the surface for derivation of the MTL equation [6].

Let us define *per-unit-length conductance,* g_{ij} S/m, between each pair of conductors as ratio of conduction current flowing between the two conductors in the transverse plane to the voltage between the two conductors. Therefore,

$$\begin{aligned}\sigma \lim_{\Delta z \to 0} \frac{1}{\Delta z} \iint_{\tilde{S}_0} \vec{\mathrm{E}}_t \cdot d\vec{\tilde{s}} &= g_{i1}(V_i - V_1) + \ldots + g_{ii} V_i + \ldots + g_{in}(V_i - V_n) \\ &= -g_{i1} V_1(z,t) - g_{i2} V_2(z,t) - \ldots \\ &\quad + \sum_{k=1}^{n} g_{ik} V_k(z,t) - \ldots - g_{in} V_n(z,t)\end{aligned} \tag{3.16}$$

Similarly, the charge per unit of line length can be defined in terms of the *per-unit-length capacitance's,* c_{ij}, between each pair of conductors as

$$\begin{aligned}\varepsilon \lim_{\Delta z \to 0} \frac{1}{\Delta z} \iint_{\tilde{S}_0} \vec{\mathrm{E}}_t \cdot d\vec{\tilde{s}} &= c_{i1}(V_i - V_1) + \ldots + c_{ii} V_i + \ldots + c_{in}(V_i - V_n) \\ &= -c_{i1} V_1(z,t) - c_{i2} V_2(z,t) - \ldots \\ &\quad + \sum_{k=1}^{n} c_{ik} V_k(z,t) - \ldots - c_{in} V_n(z,t)\end{aligned} \tag{3.17}$$

Substituting (3.15), (3.16) and (3.17) into (3.14), and dividing both sides by Δz gives

$$\frac{I_i(z+\Delta z,t) + I_i(z,t)}{\Delta z} + \sigma \frac{1}{\Delta z} \iint_{\tilde{S}_0} \vec{\mathrm{E}}_t \cdot d\vec{\tilde{s}} = -\varepsilon \frac{1}{\Delta z} \iint_{\tilde{S}_0} \vec{\mathrm{E}}_t \cdot d\vec{\tilde{s}} \tag{3.18}$$

Taking the limit as $\Delta z \to 0$ and substituting (3.16) and (3.17) yields

$$\begin{aligned}\frac{\partial I_i(z,t)}{\partial z} &= g_{i1} V_1(z,t) + g_{i2} V_2(z,t) + \ldots - \sum_{k=1}^{n} g_{ik} V_k(z,t) + \ldots + g_{in} V_n(z,t) \\ &\quad + \frac{\partial}{\partial t}\left\{ c_{i1} V_1(z,t) + \ldots - \sum_{k=1}^{n} c_{ik} V_k(z,t) + \ldots + c_{in} V_n(z,t) \right\}\end{aligned} \tag{3.19}$$

Equation (3.19) can be placed in a compact form with matrix notation giving

$$\frac{\partial}{\partial z} I(z,t) = -GV(z,t) - C\frac{\partial}{\partial t} V(z,t) \tag{3.20}$$

where V and I are given by (3.10). The *per-unit-length conductance matrix, G,* represents the *conductance current flowing between the conductors in the transverse plane* and is defined from (3.19) as

$$G = \begin{bmatrix} \sum_{k=1}^{n} g_{1k} & -g_{12} & .. & -g_{1n} \\ -g_{21} & \sum_{k=1}^{n} g_{2k} & .. & -g_{2n} \\ : & : & :: & : \\ -g_{n1} & -g_{n2} & .. & \sum_{k=1}^{n} g_{nk} \end{bmatrix} \tag{3.21}$$

The *per-unit-length capacitance matrix, C,* represents the *displacement current flowing between the conductors in the transverse plane* and is defined from (3.19) as

$$C = \begin{bmatrix} \sum_{k=1}^{n} c_{1k} & -c_{12} & .. & -c_{1n} \\ -c_{21} & \sum_{k=1}^{n} c_{2k} & .. & -c_{2n} \\ : & : & :: & : \\ -c_{n1} & -c_{n2} & .. & \sum_{k=1}^{n} c_{nk} \end{bmatrix} \tag{3.22}$$

If we denote the total charge on the i-th conductor per-unit of line length as q_i, then the fundamental definition of C is

$$Q = CV \tag{3.23a}$$

where

$$Q = \begin{bmatrix} q_1 \\ q_i \\ \vdots \\ q_n \end{bmatrix} \tag{3.23b}$$

The above per-unit-length parameter matrices once again contain all the cross-sectional dimension information that distinguishes one MTL structure from another. Although these were shown as not being symmetric, it is logical to expect that they are [6].

3.2 DERIVATION FROM THE PER-UNIT-LENGTH EQUIVALENT CIRCUIT

The MTL equation is derived from the *per-unit-length* equivalent circuit shown in Fig 3.3. Writing the Kirchoff's voltage law around the *i-th circuit* consisting of the *i*-th conductor and the reference conductor yields

$$-V_i(z,t) + r_i \Delta z I(z,t) + V_i(z+\Delta z,t) + r_0 \Delta z \sum_{k=1}^{n} I_k(z,t) \tag{3.24a}$$

$$= -l_{i1}\Delta z \frac{\partial I_1(z,t)}{\partial t} - l_{i2}\Delta z \frac{\partial I_2(z,t)}{\partial t} - \ldots - l_{ii}\Delta z \frac{\partial I_i(z,t)}{\partial t} - \ldots - l_{in}\Delta z \frac{\partial I_n(z,t)}{\partial t}$$

Dividing both sides by Δz and taking the limit as $\Delta z \rightarrow 0$ once again yields the transmission-line equation with the collection for all I given matrix form in (3.9). Similarly the second MTL equation can be obtained by applying Kirchoff's

current law to the i-th conductor in the per-unit-length equivalent circuit in Fig. 3.3 to yield

$$I_i(z+\Delta z,t)-I_i(z,t)=-g_{i1}\Delta z(V_i-V_1)-....-g_{ij}\Delta z(V_i-V_j)-.... \tag{3.24b}$$

$$-g_{in}\Delta z(V_i-V_n)-....-c_{i1}\Delta z\frac{\partial}{\partial t}(V_i-V_1)-....$$

$$-c_{ii}\Delta z\frac{\partial}{\partial t}V_i-....-c_{in}\Delta z\frac{\partial}{\partial t}(V_i-V_n)$$

Dividing both sides by Δz, taking the limit $\Delta z \to 0$, and collecting the terms once again yields the second MTL equation given in (3.20) with the collection for all i given in matrix form. Strictly speaking, the voltages in (3.24b) are at $z + \Delta z$ so that (3.24a) should be substituted before taking the limit. However, this yields the same result as when we take the limit $\Delta z \to 0$ in (3.24b) directly [6].

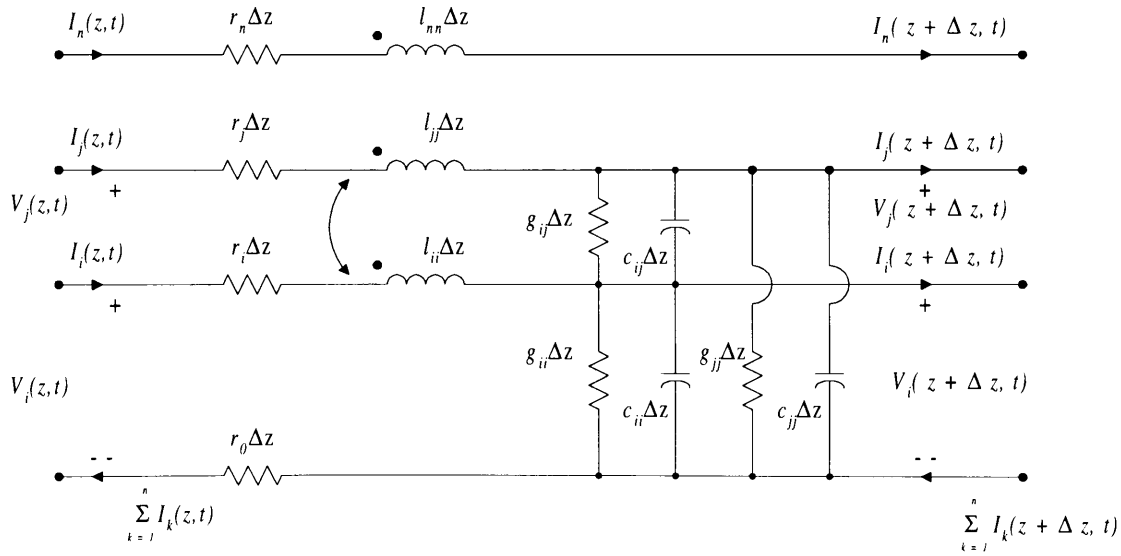

Fig. 3.3 The per-unit-length MTL model for derivation of the MTL equations [6].

3.3 Summary of the MTL Equations

The TEM-mode model of an $(n + 1)$-conductor, uniform MTL is embodied in the MTL equations as

$$\frac{\partial}{\partial z}V(z,t)+RI(z,t)+L\frac{\partial}{\partial t}I(z,t)=0 \tag{3.25a}$$

$$\frac{\partial}{\partial z}I(z,t)+GV(z,t)+C\frac{\partial}{\partial t}V(z,t)=0 \tag{3.25b}$$

where V and I are the $(n \times 1)$ vectors of the line voltages (with respect to the reference conductor) and line currents, respectively. The line cross-section dimensions are contained in the $(n \times n)$ per-unit-length parameter matrices of R (resistance), L (inductance), G (conductance), and C (capacitance).The position along the line is denoted as z and time is denoted as t [16]. The MTL equations in (3.25) are a set of $2n$, *coupled, first-order, partial differential equations*. They may be put in a more compact form as [6]

$$\frac{\partial}{\partial z}\begin{bmatrix}V(z,t)\\ I(z,t)\end{bmatrix}=-\begin{bmatrix}0 & R\\ G & 0\end{bmatrix}\begin{bmatrix}V(z,t)\\ I(z,t)\end{bmatrix}-\begin{bmatrix}0 & L\\ C & 0\end{bmatrix}\frac{\partial}{\partial t}\begin{bmatrix}V(z,t)\\ I(z,t)\end{bmatrix} \tag{3.26}$$

This first order form is especially helpful when we set out to solve them. If the conductors are perfect conductors, PEC, R=0, whereas if the surrounding medium is lossless ($\sigma = 0$), G=0. The line is said to be *lossless*, in which case the MTL equations simplify to

$$\frac{\partial}{\partial z}\begin{bmatrix}V(z,t)\\ I(z,t)\end{bmatrix}=-\begin{bmatrix}0 & L\\ C & 0\end{bmatrix}\frac{\partial}{\partial t}\begin{bmatrix}V(z,t)\\ I(z,t)\end{bmatrix} \tag{3.27}$$

The frequency-domain analysis of uniform MTL is a straight forward computational task whether the line is considered lossless or lossy. The time-domain analysis of lossy MTL's is considered more difficult for several reasons. A primary reason is that the resistive losses of the conductors are due to skin effect and vary with frequency as $\sqrt{f}$. The representation of this frequency dependence in the time domain is a convolution which presents computational problems in a direct, time-domain solution of the MTL equations. These problems have led to the use of other solution methods for the time-domain analysis of lossy MTL's. One of the important approximation solution techniques is the FDTD method. For MTL, a two dimensional, 2D, FDTD algorithm is applied. The line axis z is discretized in Δz increments or spatial cells, the time variable t is discretized in Δt increments or temporal cells, and the derivative in the MTL equations are approximated by finite difference. The solution voltages and currents are obtained at these discrete points and represent an approximate solution of the MTL equations. In general, the accuracy of the solution depends on having sufficiently small spatial and temporal cells. Anyhow, very small spatial and temporal cells lead to high computational cost. The FDTD method has been used successfully to solve more general electromagnetic problems, wherein lossy, nonlinear, and/or inhomogeneous media may be considered. The spatial and temporal independent variables of the time-domain Maxwell's

equations are similarly discretized, and the boundary conditions are readily incorporated.

MTL's are simply one-dimensional versions of wave propagation embodied in the three-dimensional Maxwell's equations for the special case of the TEM or quasi-TEM mode of propagation. An important difference in the boundary condition. For the full-wave electromagnetic problem, zero tangential electric field on the surface of perfect conductors is a primary boundary condition. Scattering problems can be handled with the ABC. In the case of MTL's, the boundary conditions are lumped loads at the two ends of the line, z = 0 and $z = l$ where l is the length of the MTL. Linear, resistive termination's can be characterized by generalized Thevenin Equivalents as [16]

$$V(0,t) = V_S - R_S I(0,t) \tag{3.28a}$$

$$V(l,t) = V_L - R_L I(l,t) \tag{3.28b}$$

or a similar generalized Norton Equivalent or a combination of the two. In order to insure stability in the FDTD solution, the discrete voltage and current solution points are not physically located at the same point but are staggered one-half cell apart. However, the lumped terminal constraints such as in (3.28) require that the current and voltage solution points be collocated [6].

Chapter 4

Time-Domain Analysis

4. TIME - DOMAIN ANALYSIS

In this chapter, two cases of MTL models are analyzed. First case is a two-conductor MTL and the second a three-conductor MTL. In both cases, the models are lossless. The total solution of the MTL equations for general time variation of the sources is presented. This solution include both the transient and the steady state components of the solution.

4.1 CASE I, TWO - CONDUCTOR MTL

The transmission line is a two-conductor lossless MTL. The length of the line is 100 meters and the characteristic inpedance Z_0 = 100 Ω. The DC generator at the near-end of the transmission line has a resistance R_G = 20 Ω and generates a pulse of magnitude 10V. The excitation source has a rise and fall time of 15 ns and a pulse width of 100 ns. The final solution time is 1600 ns. The load resistance R_L = 200 Ω (see Fig 4.1). As a pulse is sent along the line, discontinuities on the line reflect waves back (echoes). The voltage reflection coefficients are given by

$$\rho_L = \frac{(R_L - R_0)}{(R_L + R_0)} \tag{4.1a}$$

$$\rho_G = \frac{(R_G - R_0)}{(R_G + R_0)} \tag{4.1b}$$

where ρ_L is the voltage reflection coefficient of load and ρ_G is the voltage reflection coefficient of generator. The electrical schematic of the transmission line is shown in Fig. 4.1. [8].

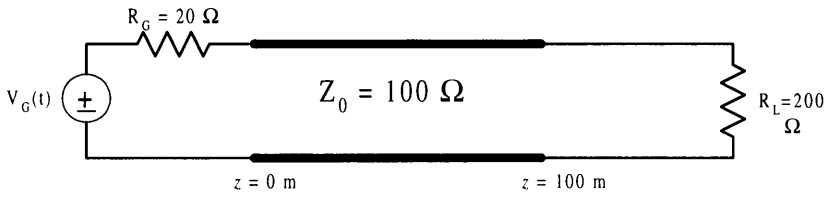

Fig. 4.1 Electrical schematic of two-conductor MTL, 100 m long with a pulse generator of internal resistance 20 Ω and 200Ω load resistance. The characteristic impedance of the line is 100Ω [8].

4.1.1 COMPUTED RESULTS

In this model, a trapezoidal pulse of rise and fall time 15 ns and a pulse width of 100 ns is used as the excitation pulse. The first step is to find *f*, which is given by

$$f = \frac{1}{\pi \times \tau_r} \tag{4.2}$$

where τ_r is the rise time of the pulse. For a rise time of 15 ns, we get f = 21.2 MHz. Let λ be the wavelength of the wave, which is represented by

$$\lambda = \frac{c}{f} \tag{4.3a}$$

$$c = \sqrt{\frac{1}{\mu \varepsilon}} \tag{4.3b}$$

where c is the velocity of propagation, f is the frequency, μ is the permeability of the surrounding medium and ε is the permittivity of the surrounding medium. For free space, $\mu_0 = 4\pi \times 10^{-7}$ H/m and $\varepsilon_0 \approx (1/36\pi) \times 10^{-9}$ F/m . In general c_0 is taken as 3×10^8 ms^{-1}, the speed of light. Upon calculation, the wavelength is

$$\lambda = \frac{3 \times 10^8}{21.2 \times 10^6} = 14.137 \text{ m}$$

For simulation, we should make λ electrically short. This is done by dividing λ by 10, which gives $\lambda_{short} = \frac{\lambda}{10}$ =1.4137 m. Δz, the spatial cell, should be less than or equal to λ_{short}. Let Δz = 1 m.

After calculating the size of the spatial cell, one has to calculate the number of spatial cells Δz needed and the number of time steps Δt needed to run the simulation. The number of spatial cells needed, *NDZ*, is given by

$$NDZ = \frac{\text{length of line}}{\Delta z} \tag{4.4}$$

By calculation, NDZ = 100. After finding NDZ, the number of time step NDT is found, which is given by

$$NDT = \frac{\text{final solution time}}{\Delta t} \tag{4.5}$$

where Δt, is the time step, given by

$$\Delta t \leq \frac{\Delta z}{c} \tag{4.6}$$

Calculating, we get Δt = 3.3 ns.

In this model, the final solution time is 1600 ns, which makes NDT = 480. One of the conditions for calculating NDZ and NDT is that, it should satisfy the Courant stability condition [6], given by

$$NDT \geq NDZ \frac{c \times \text{ final solution time}}{l} \tag{4.7}$$

where l is the length of the transmission line and c is the velocity of propagation.

In this model, a ribbon cable is considered as the transmission line. The radius of the ribbon cable is chosen to be 7.5 mils. Another important task is to find the distance between the two conductors (center to center). It should be noted that the characteristic impedance of the transmission line depends on the radius of the wires and the distance between them (center to center). The characteristic impedance Z_0 is given by

$$Z_0 = \frac{\eta}{\pi} \cosh^{-1} \frac{d}{a} \tag{4.8}$$

where η is the intrinsic impedance of the dielectric medium = $\eta_0 = \sqrt{\frac{\mu_0}{\varepsilon_0}} =$ 376.731 $\Omega \approx 120 \times \pi$ [3], a is the radius of the conductors and $2d$ is the distance between the conductors, center to center (see Fig. 4.2). Upon calculation, we get the distance between the wires equal to 20.5168 m. Shengyao Hu [24] has used FDTD method for the analysis of ribbon cable.

From the values of a and D, the per-unit-length parameters for this ribbon cable model are computed using the program RIBBON.FOR [6].

$L = 0.33333\ \mu H$

$C = 33.3795\ pF$

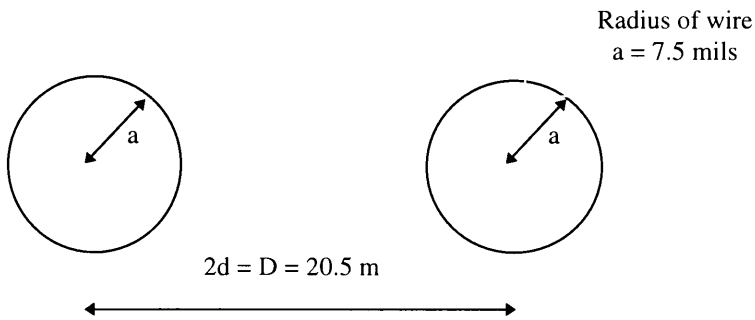

Fig. 4.2 End-on view of structure of two-conductor MTL.

The characteristic impedance Z_0 of the MTL (for lossless condition) is given by

$$Z_0 = \sqrt{\frac{L}{C}} = R_0 \qquad (4.9)$$

Cross checking, the computed values of L and C satisfies equation (4.9). Also for lossless lines in a homogeneous media, there is an important identity

$$LC = \mu\varepsilon \tag{4.10a}$$

If we have a ($n + 1$) conductor transmission line, then the per-unit-length parameters will be a ($n \times n$) matrix. Equation (4.10a), can be represented as

$$C = \mu\varepsilon L^{-1} \tag{4.10b}$$

With these per-unit-length values of L and C, the FDTD code, FINDIF.FOR [6] is executed.

The results of the FDTD simulation are shown in Fig. 4.3 and Fig. 4.4. The model is analyzed at two locations in the transmission line. The near-end (Fig. 4.3) is the side of the MTL near the source (generator). The far-end (Fig. 4.4) is at the end of the MTL, near the load resistance.

4.1.2 VALIDATION

The computed results from FDTD method was validated with 2 different results. The first is an analytical simulation, based on BASIC program presented by Kraus [8]. The second is a SPICE simulation. The SPICE code used for this simulation is given in Appendix A, Table 1.1.

4.1.2.1 ANALYTICAL SIMULATION

A simple BASIC program [8] was used for this simulation. The near-end voltage is plotted as shown in Fig. 4.5. Similarly, the far-end voltage is plotted as shown in Fig. 4.6. As can be seen, the FDTD plots, for both near-end and far-end voltages, are very much in agreement with the analytical plots shown in Fig. 4.5 & Fig. 4.6.

4.1.2.2 SPICE SIMULATION

In this simulation, the two-conductor MTL is represented in a SPICE model. The values of L and C are taken from above. The command to represent a transmission line in SPICE simulation is

```
T1 5 0 6 0 Z0=9.993076E+01 TD=3.335639E-07
```
(4.11)

where `Z0` is the characteristic impedance of the line and `TD` is the time delay. The starting point of the MTL is node 5 and the end point is node 6. Node 0 is, naturally, the ground point. The near-end voltage is plotted and given in Fig. 4.7 while the far-end is given in Fig. 4.8.

As can be seen from Fig 4.3 to Fig. 4.8, the results agree very much among each other. For a single plot comparison, all the three sets of near-end voltages are plotted in Fig. 4.9. Likely, all the far-end voltages are plotted in Fig. 4.10.

From these two figures, it can be concluded that the results are very very close to each other.

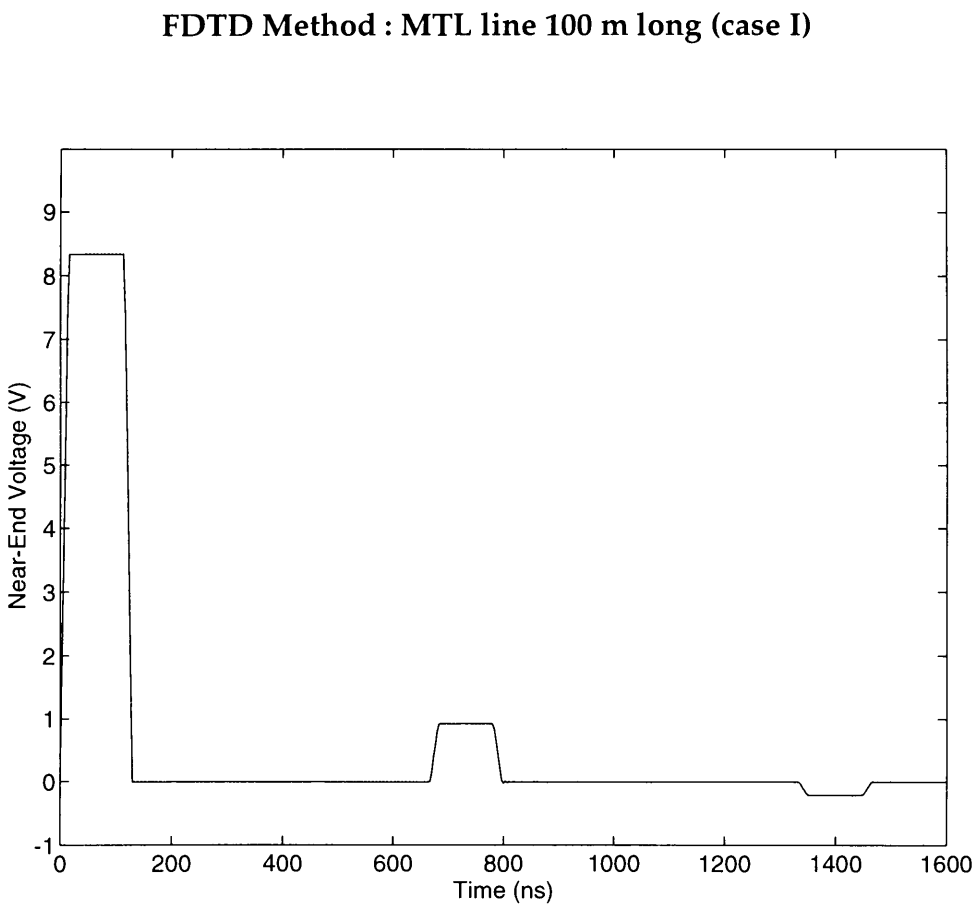

Fig. 4.3 Near-End voltage for two-conductor MTL using FDTD method. The length of the line is 100 m and *NDZ*=100 and *NDT*=480 [Author].

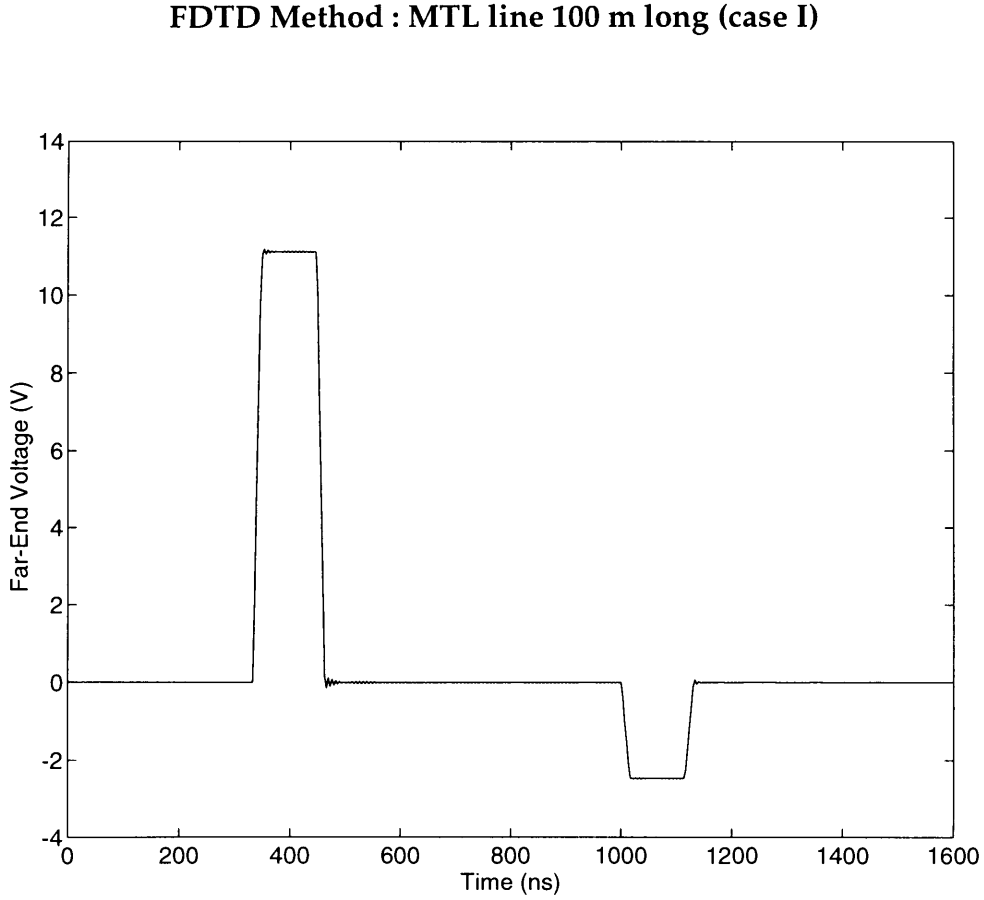

Fig. 4.4 Far-End voltage for two-conductor MTL using FDTD method. The length of the line is 100 m and *NDZ*=100 and *NDT*=480 [Author].

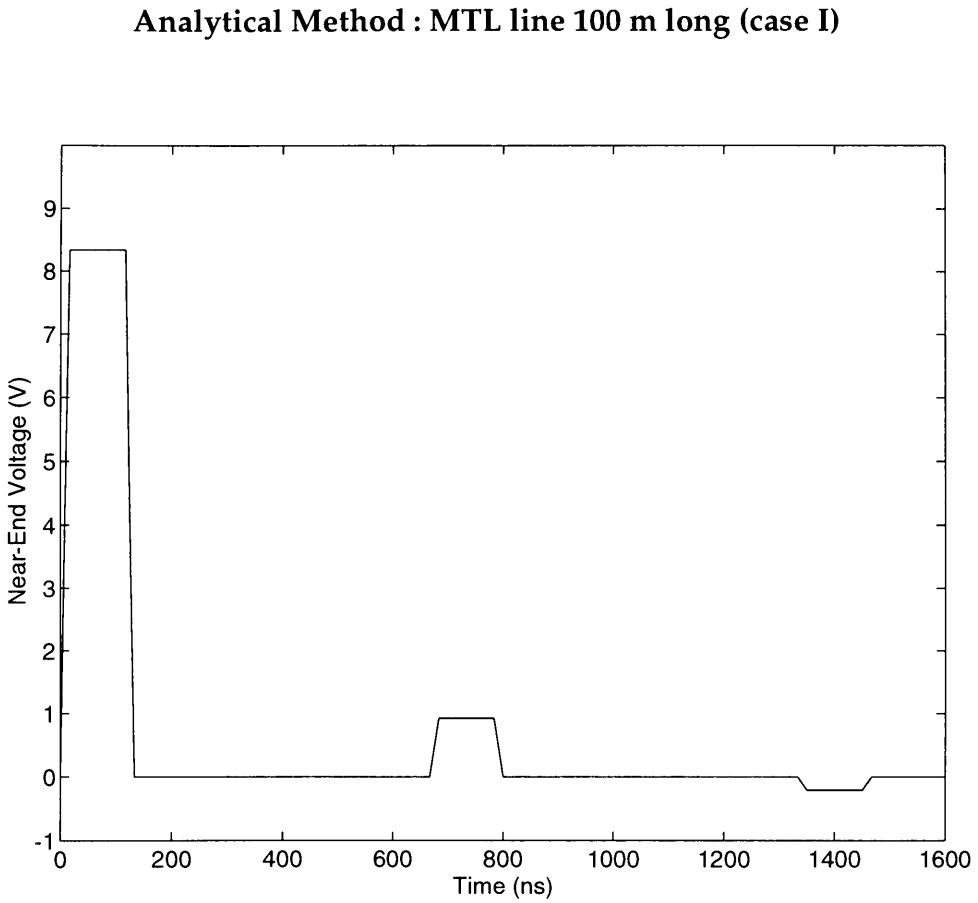

Fig. 4.5 Near-End voltage for two-conductor MTL using analytical method. The length of the line is 100 m [8].

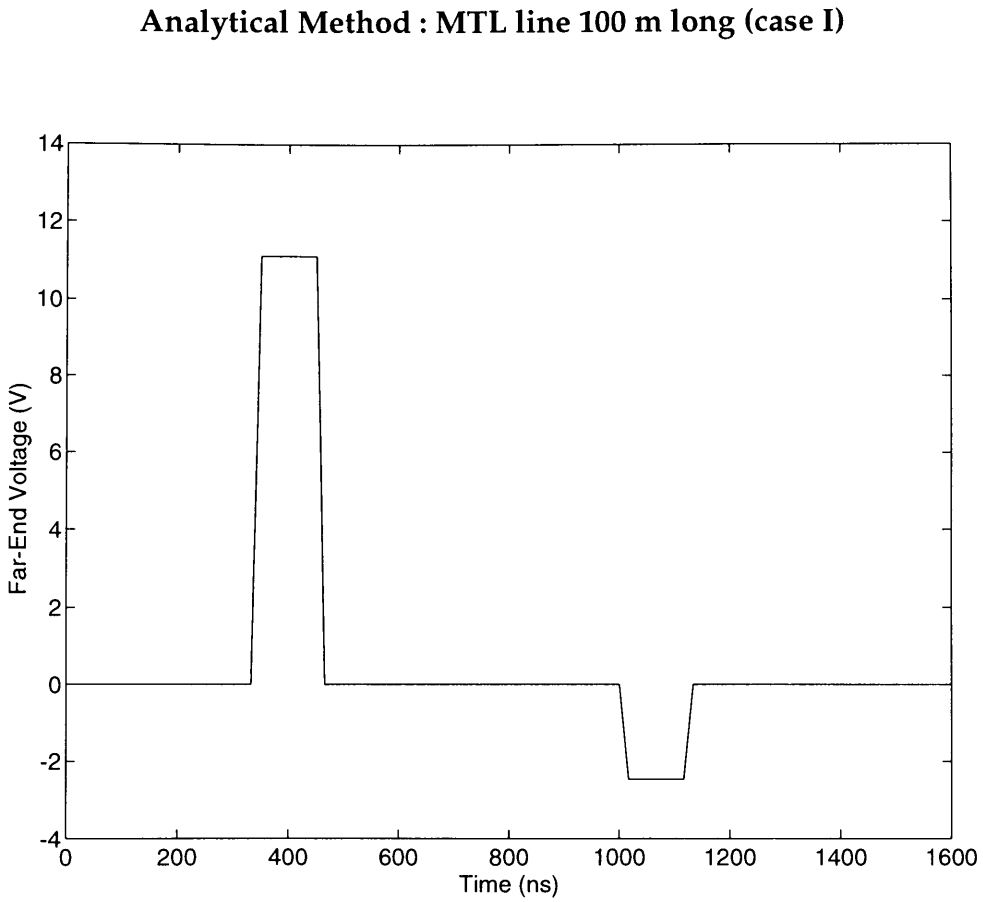

Fig. 4.6 Far-End voltage for two-conductor MTL using analytical method. The length of the line is 100 m [8].

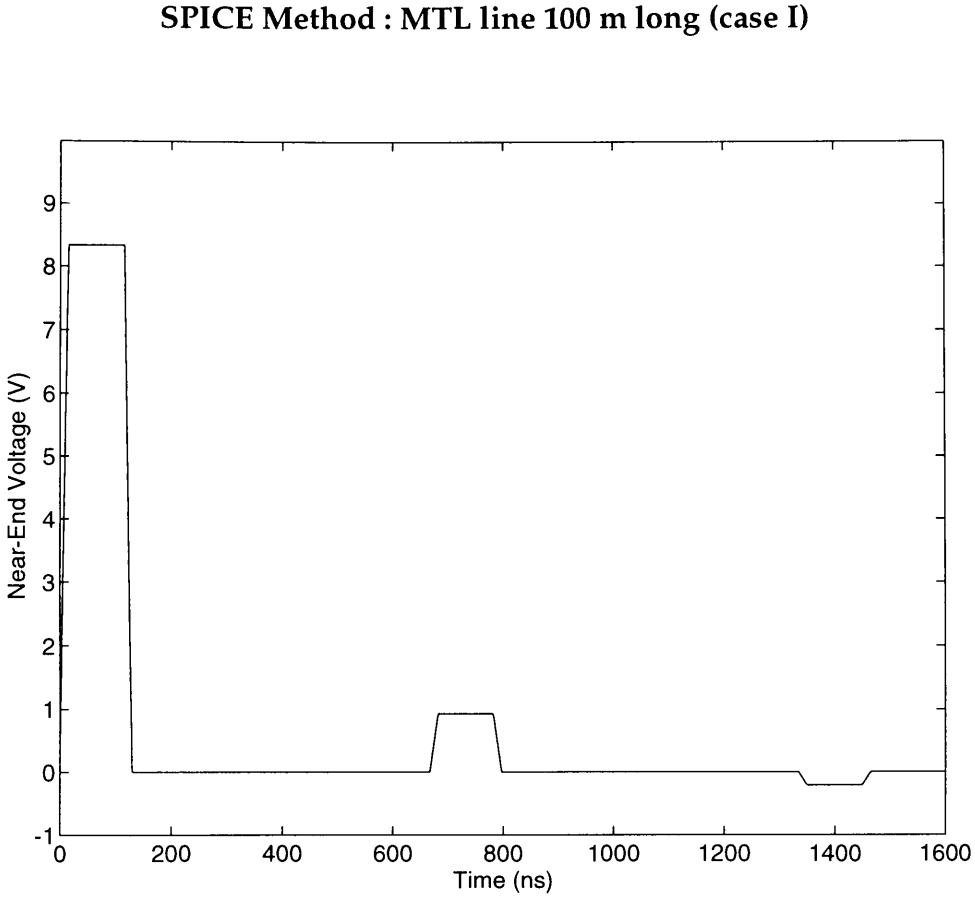

Fig. 4.7 Near-End voltage for two-conductor MTL using SPICE method. The length of the line is 100 m and the time delay for the line is 33.3 μs [Author].

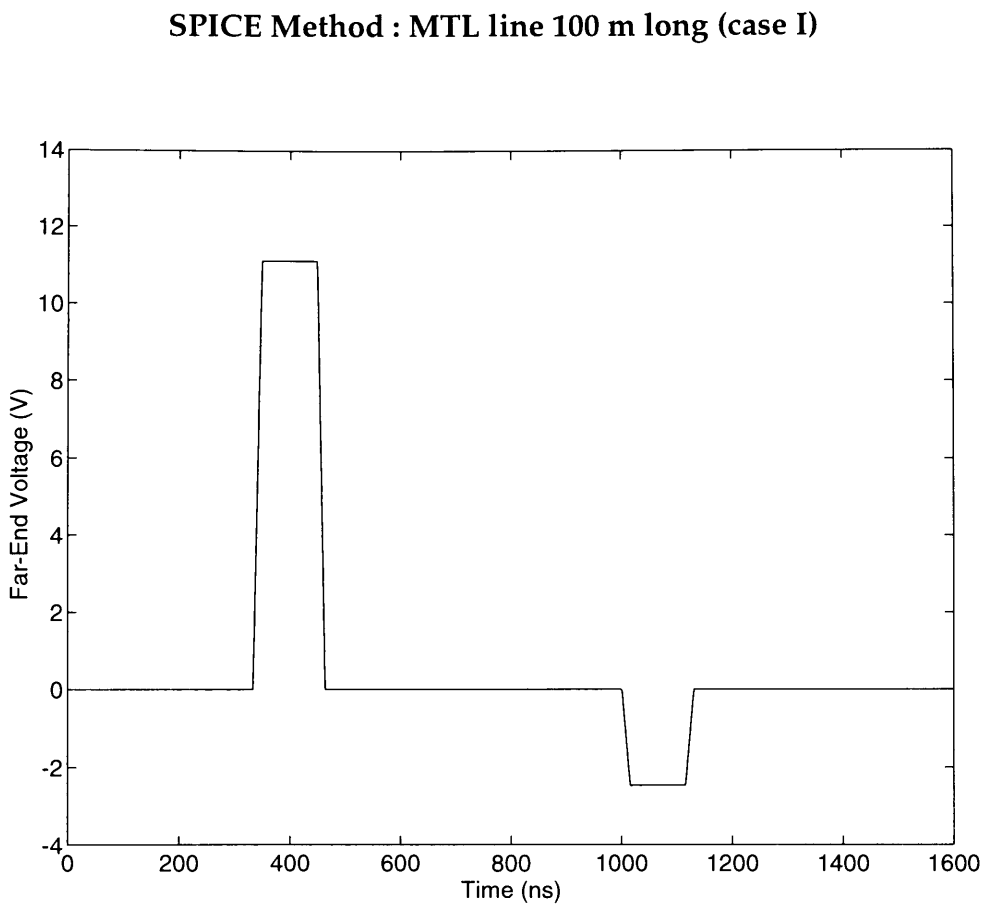

Fig. 4.8 Far-End voltage for two-conductor MTL using SPICE method. The length of the line is 100 m and the time delay for the line is 33.3 μs [Author].

FDTD Method [Author], Analytical Method [8] & SPICE Method [Author]

(case I)

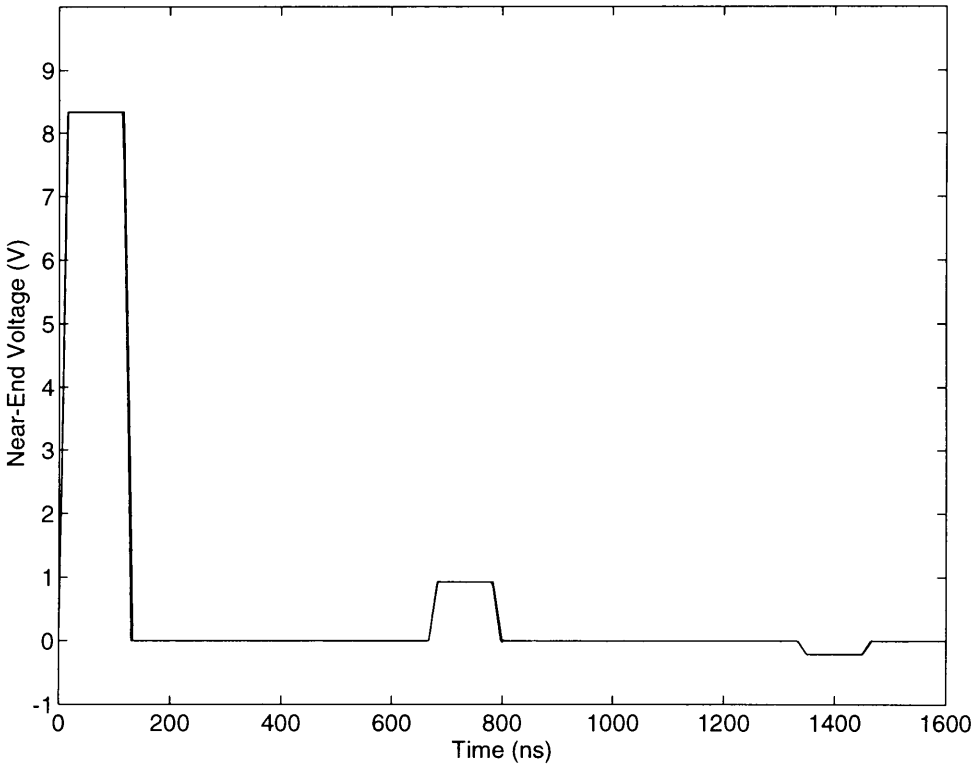

Fig. 4.9 Near-End voltages for two-conductor MTL using FDTD, analytical and SPICE method. The length of the line is 100 m.

FDTD Method [Author], Analytical Method [8] & SPICE Method [Author]

(case I)

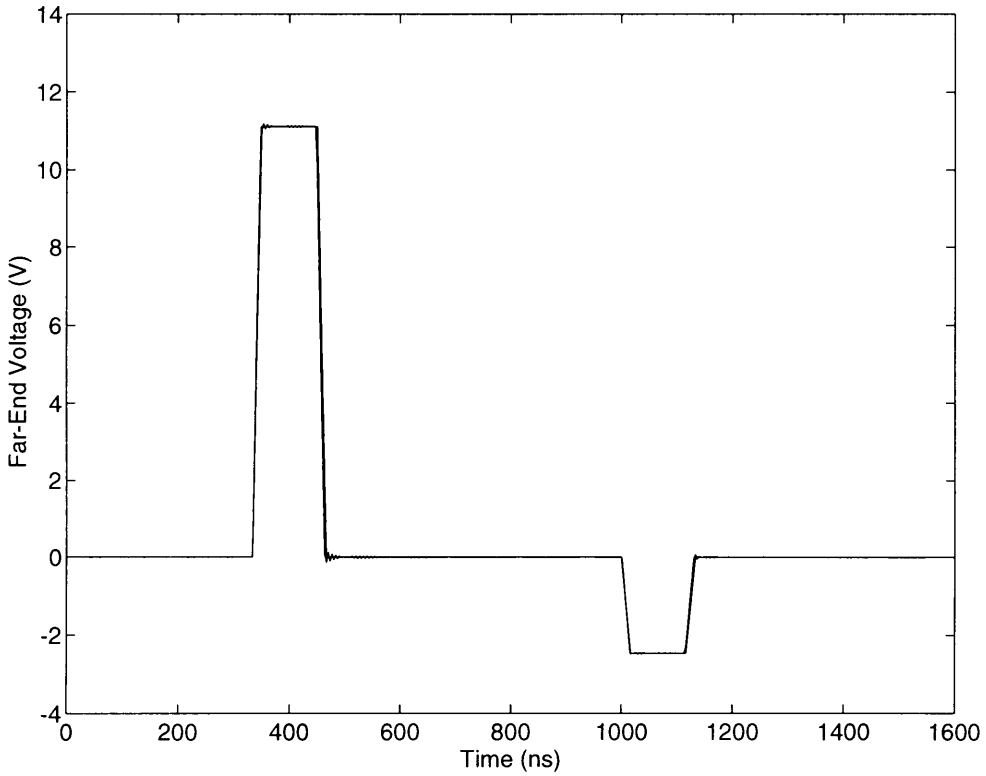

Fig. 4.10 Far-End voltages for two-conductor MTL using FDTD, analytical and SPICE method. The length of the line is 100 m.

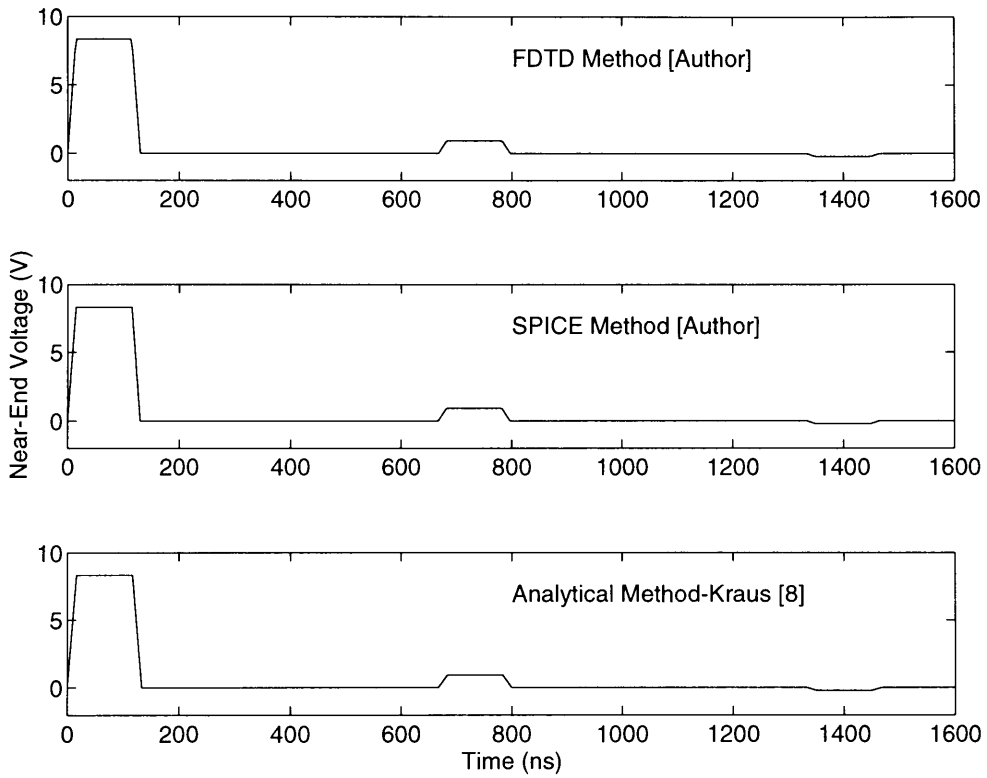

Fig. 4.11 Near-End voltages for two-conductor MTL using FDTD, analytical and SPICE method in subplot setup. The length of the line is 100 m.

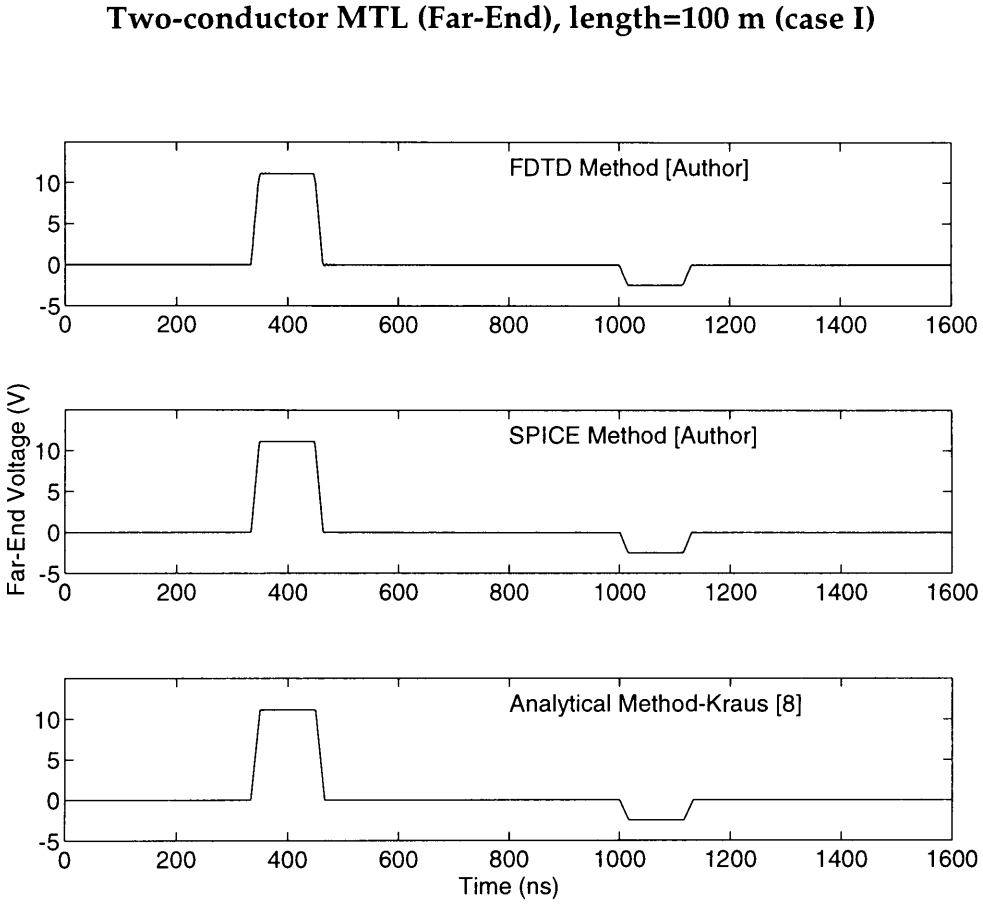

Fig. 4.12 Far-End voltages for two-conductor MTL using FDTD, analytical and SPICE method in subplot setup. The length of the line is 100 m.

In fact they are so close that, over most of the time period, they are over lapping each other. A second approach of evaluation is to plot all the three sets of data in rows, below each other (sub plots), and to make sure under the same scale. Fig 4.11 and Fig. 4.12 are presented for comparison study of near-end and far-end voltages, respectively.

4.2 CASE II, THREE - CONDUCTOR MTL

Here a three-conductor MTL is analyzed. In this MTL, the only propagation modes are TEM or quassi-TEM. For validation of the FDTD method, a SPICE model with a network of two-wire delay lines are used which represents an MTL with *homogeneous* dielectric [5].

4.2.1 COMPUTED RESULTS

The three-conductor MTL model is represented as two conductors above a perfectly conducting ground plane. The conductors are standard 20 Gauge wires with a radius of 0.41 mm. The distance between the conductors is 20 mm (center to center) and both the conductors are 20 mm above the ground plane. The transmission line is 4.67 meters long. The excitation pulse is a trapezoidal pulse with rise and fall time of 12.5 ns and a pulse width of 7.5 ns. The final time is 200

ns and the magnitude is 1V. Conductor One has a source resistance R_S = 50 Ω and a load resistance R_L = 50 Ω. The excitation pulse is given in this conductor. The second conductor has a near-end resistance R_{NE} = 50 Ω and a far-end resistance R_{FE} = 50 Ω. An end-on view of the structure is given in Fig. 4.13.

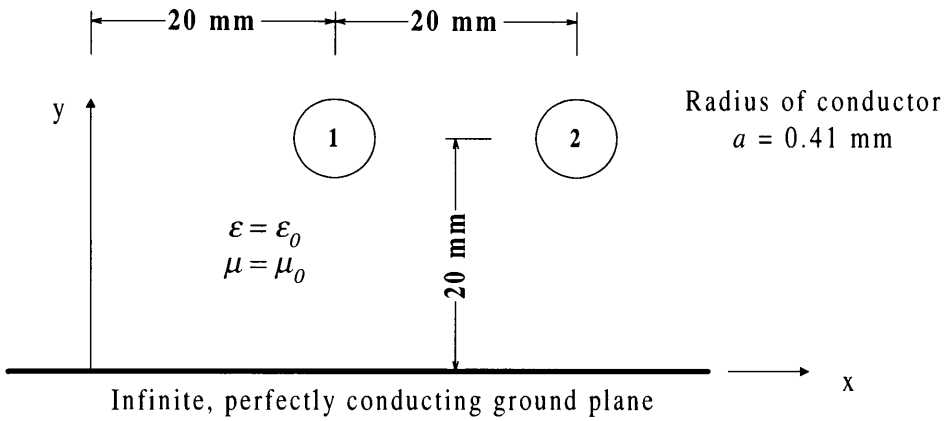

Fig. 4.13 End-on view of structure of three-conductor MTL above an infinite, perfectly conducting ground plane [5].

The second conductor is used to collect the near-end and far-end voltage for analysis. An electrical schematic diagram of the MTL is given in Fig. 4.14.

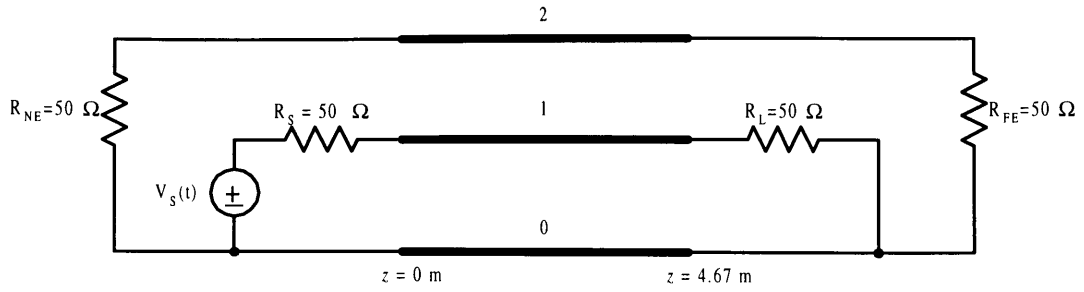

Fig. 4.14 Electrical schematic of three-conductor MTL, 4.67 m long with a pulse generator of internal resistance 50 Ω at the source and a 50Ω load resistance. The near-end resistance is 50Ω and the far-end resistance is 50 Ω [5].

Upon calculation for the per-unit-length parameters, the values of L and C are computed as

$$L = \begin{bmatrix} 0.9129 & 0.1609 \\ 0.1609 & 0.9129 \end{bmatrix} \quad \mu\text{H}$$

$$C = \begin{bmatrix} 12.5787 & -2.2176 \\ -2.2176 & 12.5787 \end{bmatrix} \quad p\text{F}$$

These values of L and C are computed using the program WIDESEP.FOR [6] which are used as input data for the FDTD program, FINDIF.FOR [6]. In this model, we are interested in the near-end voltage on conductor number two.

For the simulation, we have to find out the values of Δz, Δt, NDZ and NDT. The procedure is the same as previously done for case I model (two-conductor MTL).

Using (4.2) and (4.3), λ = 11.78 m. Hence λ_{short} = 1.178 m. Δz is chosen at 0.778 m which gives *NDZ* = 6, according to (4.4). Using (4.6) Δt = 2.59 ns. We choose Δt as 2 ns, which gives *NDT* = 100 (4.5). So the simulation is run for Δz = 0.778, Δt = 2 ns, *NDZ* = 6 and *NDT* = 100. The results of this simulation is given in Fig. 4.16c. This result is very much in agreement with the SPICE results [5].

In order to investigate the possibility of better result, different *NDZ* and *NDT* combinations are evaluated. Table 4.1 gives a comparative study of different combinations of *NDZ* and *NDT* simulated.

Δz	*NDZ*	Δt (ns)	*NDT*	Result
1.167	4	3.33	60	Good
1.167	4	2	100	Satisfactory
.778	6	2	100	Good

Table 4.1 Comparative table for FDTD simulations for different values of *NDZ* and *NDT* for two-conductor MTL.

As can be seen from Table 4.1 and Fig. 4.16, any change in *NDZ* or *NDT*, there are slight changes in the near-end voltage on conductor two. Anyhow, the best result is observed for *NDZ* = 6 and *NDT* = 100. The near-end voltages for

various *NDZ* and *NDT* are given in Fig 4.16 with respect to the validation model, in this case, a SPICE simulation.

4.2.2 VALIDATION

The validation is based on the simulation presented by Marx *et al* [5]. Marx has successfully represented an MTL with a network of two-wire delay lines. In the proceeding chapter, two-wire delay-lines, as equivalent to MTL, is presented.

4.2.2.1 SPICE SIMULATION

Signals on the line consists of waves which propagate in forward and backward directions on the line with velocity of propagation c (4.3b). For these waves, the currents and voltages are related by

$$I_f = Y_0 V_f \tag{4.12}$$

$$I_b = -Y_0 V_b \tag{4.13}$$

where subscripts f and b refer to forward and backward traveling waves, respectively, and Y_0 is the characteristic admittance matrix, and Z_0 is the characteristic impedance matrix [2], given by:

$$Y_0 = cC \tag{4.14}$$

$$Z_0 = Y_0^{-1} \tag{4.15}$$

Presented below is a system of two-wire lines that is an exact synthesis of the MTL shown in Fig. 4.14.

It is assumed that there is an infinitely long MTL. Then any n-port source connected to it sees a purely resistive n-port network with admittance matrix Y_0. This suggests that one can simulate the MTL with a system of two-wire lines, one for each pair of ports with characteristic impedance chosen so that the admittance matrix is just Y_0. This arrangement is shown schematically in Fig 4.15.

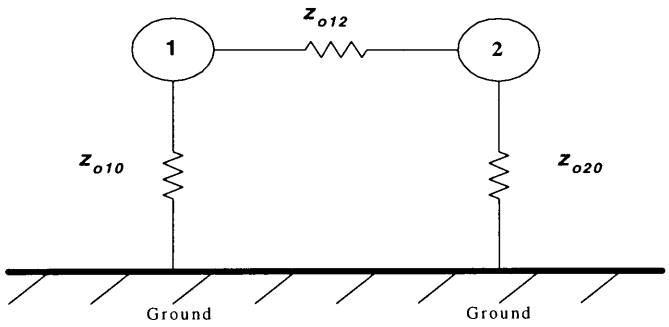

Fig. 4.15 Representation of the synthesis of a three-conductor transmission line with three two-wire lines. An end-on view of two wires over a ground plane is shown. The resistance $z_{0_{\alpha\beta}}$ represents the characteristic impedance of the two-wire line connected between conductor α and conductor β [5].

In general, the number m of two-wire lines required is

$$m = \frac{n(n-1)}{2} \tag{4.16}$$

where n is the number of conductors in the MTL, in our case, three. The line connecting conductor α to conductor β will be designated $T_{\alpha\beta}$ with characteristic impedance $z_{o_{\alpha\beta}}$ (ground is conductor 0).

It is easy to select the $z_{o_{\alpha\beta}}$ so that the admittance matrix is Y_0. The matrix has the following properties. It is real, symmetric, dominant, and has positive diagonal elements and negative off-diagonal elements. Let the elements be $Y_{0_{\alpha\beta}}$. By definition, $Y_{0_{\alpha\beta}}$ is the current flowing into the conductor α per unit voltage applied to conductor β with all the conductors other than β shorted to ground. The network of $z_{o_{\alpha\beta}}$ will satisfy these requirements if one chooses

$$z_{o\alpha\beta} = -\frac{1}{Y_{o\alpha\beta}}, \qquad \alpha \neq \beta \ , \ \beta \neq 0 \tag{4.17}$$

$$z_{o\alpha 0} = \frac{1}{\sum_{\beta=1}^{n-1} Y_{o\alpha\beta}} \tag{4.18}$$

where the sum is over all conductors including the αth conductor. Recall that $Y_{0_{\alpha\beta}}$ is real and negative if $\alpha \neq \beta$. Then as evaluated in (4.17), $z_{o_{\alpha\beta}}$ is real and positive and can be realized with an ideal time delay. Furthermore, $Y_{0_{\alpha\alpha}}$ is positive and Y_0 is dominant. Hence the sum in (4.18) is positive , and $z_{o_\alpha 0}$ is similarly realizable.

This result for an MTL of infinite length suggests that *finite-length* MTL with homogeneous dielectric can be simulated with m two-wire lines of the same

length and propagation of velocity, where m is given by (4.16) and the characteristic impedances are given by (4.17) and (4.18).

From the values of L and C, we find the characteristic admittance Y_0 and characteristic impedance Z_0 of the MTL, which are

$$Y_0 = \begin{bmatrix} 3.747 & -0.657 \\ -0.657 & 3.747 \end{bmatrix} \quad \text{m mho}$$

$$Z_0 = \begin{bmatrix} 275.3454 & 48.2791 \\ 48.2791 & 275.3454 \end{bmatrix} \quad \Omega$$

$$z_{o12} = -\frac{1}{Y_{o12}} = \frac{-1}{-0.657\times 10^{-3}} = 1522 \ \Omega$$

$$z_{o10} = \frac{1}{\sum_{\beta=1}^{2} Y_{o1\beta}} = \frac{1}{Y_{o11}+Y_{o12}} = \frac{1}{3.747\times 10^{-3}+(-0.657\times 10^{-3})}$$

$$z_{o10} = z_{o20} = 323.6 \ \Omega$$

The SPICE code used for the simulation is given in Appendix A Table 1.2. The time delay for the SPICE model is given by

$$t_d = \frac{d}{c_0} \tag{4.19}$$

for d = 4.67 m and $c_0 = 3 \times 10^8$, we get t_d = 15.56 ns. The resulting SPICE output is used for validation of FDTD method and is given in Fig. 4.16.

Three-conductor MTL : FDTD and SPICE Method (case II)

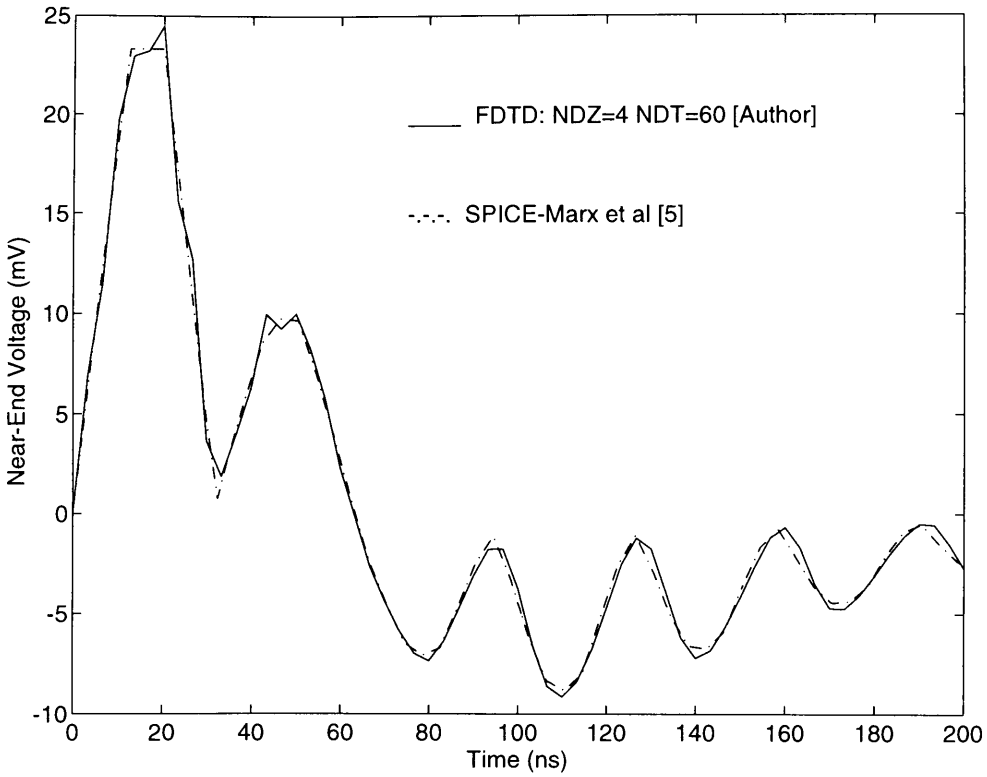

Fig. 4.16a Near-End voltages for three-conductor MTL using FDTD and SPICE method. The length of the line is 4.67 m. *NDZ*=4 and *NDT*=60. Data is recorded on the second conductor.

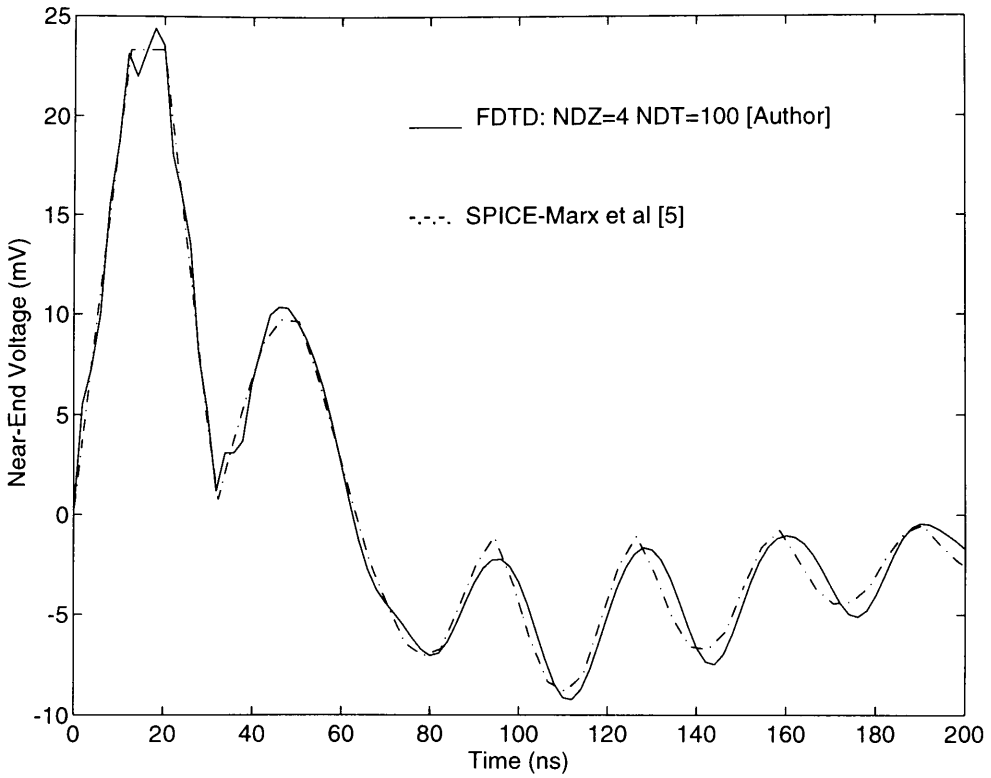

Fig. 4.16b Near-End voltages for three-conductor MTL using FDTD and SPICE method. The length of the line is 4.67 m. *NDZ*=4 and *NDT*=100. Data is recorded on the second conductor.

Three-conductor MTL : FDTD and SPICE Method (case II)

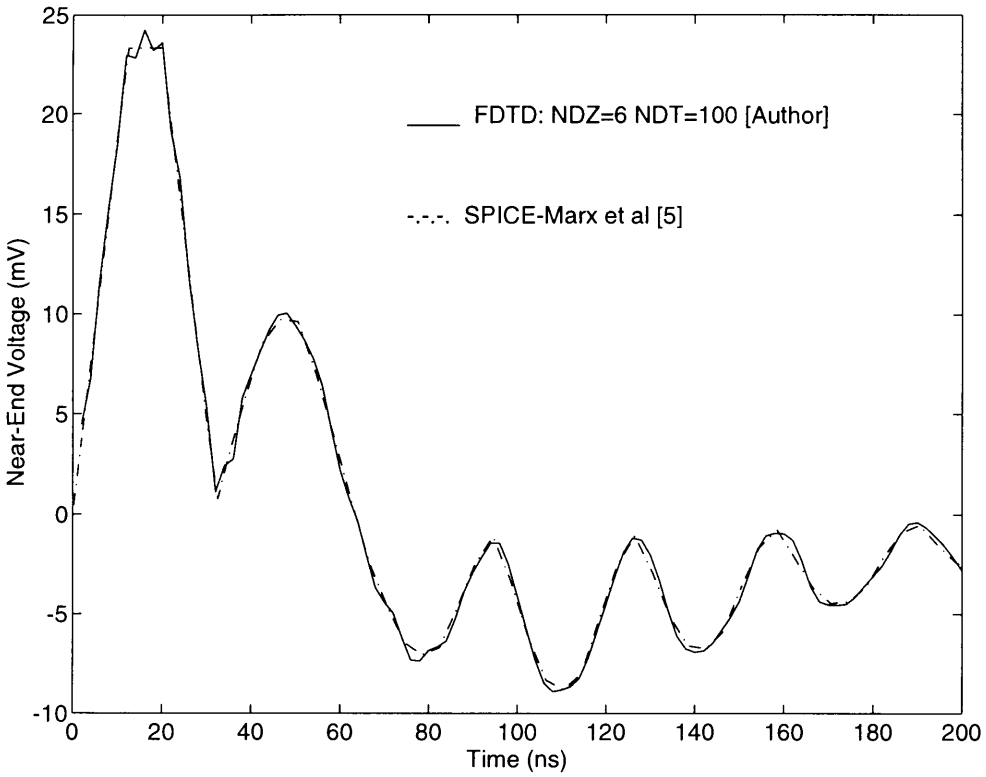

Fig. 4.16c Near-End voltages for three-conductor MTL using FDTD and SPICE method. The length of the line is 4.67 m. *NDZ*=6 and *NDT*=100. Data is recorded on the second conductor.

Chapter 5

Frequency-Domain Analysis

5 FREQUENCY - DOMAIN ANALYSIS

Here the frequency-domain analysis of a three-patch microstrip coplanar parasitic antenna array is presented. A three-dimensional, 3D, FDTD code [3] is used for the simulation. As can be seen from case I and case II models, the data computed are initially in the time-domain. Then Fourier transformation is implemented to obtain the frequency components of the signal in time-domain.

5.1 FOURIER TRANSFORM

In order to compute the Fourier spectrum of a signal by means of a digital computer, the time-domain signal must be represented by sample values, and the spectrum must be computed at a discrete number of frequencies. It can be shown that the following sum gives an approximation to the Fourier spectrum of a signal at frequencies $\frac{k}{NT_s}$

$$X_k = \sum_{n=0}^{N-1} x_n e^{-j\frac{2\pi}{N}nk} \qquad (5.1)$$

where k = 0, 1, 2 ...., N-1 and x_0, x_1, x_2 .....x_{N-1} are N sample values of the signal taken at T_s-second intervals for which the Fourier spectrum is desired. The sum (5.1) is called the *discrete Fourier transform (DFT)* of the sequence $\{x_n\}$. According to the sampling theorem, if the samples are spaced by T_s seconds, the spectrum repeats every $f_s = T_s^{-1}$ Hz. Since there are N frequency samples in this interval, it follows that the frequency resolution of (5.1) is $\frac{f_s}{N} = \frac{1}{NT_s} \equiv \frac{1}{T}$.

A little thought will indicate that to compute the complete DFT spectrum of a signal, approximately N^2 complex multiplication's are required in addition to a number of complex additions. It is possible to find algorithms that allow the computation of the DFT spectrum of a signal using only approximately $N \text{Log}_2 N$ complex multiplications. Such algorithms are referred to as *fast Fourier transform (FFT) algorithms* [20].

MATLAB, a commercial software, is used for this transformation. `fft(x)` is the discrete Fourier transform of vector `x`, computed with a fast Fourier transform (FFT) algorithm. If `x` is a matrix, `fft(x)` is the FFT of each column of the matrix. If the length of `x` is a power of two, a fast radix-2 fast Fourier transform algorithm is used. If the length of `x` is not a power of two, a slower non-power-of-two algorithm is employed. `fft(x,n)` is the n-point `fft`, padded with zeros if `x` has less than `n` points and truncated if it has more [21].

5.2 CASE III - MICROSTRIP PARASITIC ARRAY

Under frequency-domain analysis, a microstrip antenna is analyzed. The model is a three-patch microstrip coplanar parasitic antenna array (Fig. 5.1 and Fig. 5.2). The elements are rectangular in shape with the center element fed by an offset microstrip line and outer elements parasitically coupled to the center element [15].

The code used for the simulation is based on Kunz [3]. Kunz put forward a three-dimensional, 3D, FDTD code based on the formulation of Yee cell cube (Fig 2.1). This code can build simple shapes such as rectangular blocks, planes, wires, spheres and cylinders. The first-order Mur's ABC is used in the code. The source excitation is a Gaussian pulse.

The microstrip line is intended to have an impedance of 50 Ω (59 mils width). Modeling the microstrip with a half-cell correction (i.e., the line was modeled as being $\frac{1}{2}$ cell narrower than the actual physical dimension) led to the calculation of Z_0 = 50.98 - j7.2 Ω and ε_{eff} = 1.91 at 3.35 GHz. This compares well to the figure of ε_{eff} = 1.904 at 4.0 GHz listed for a 50 Ω line on this substrate in the RT/Duroid product information manual [15].

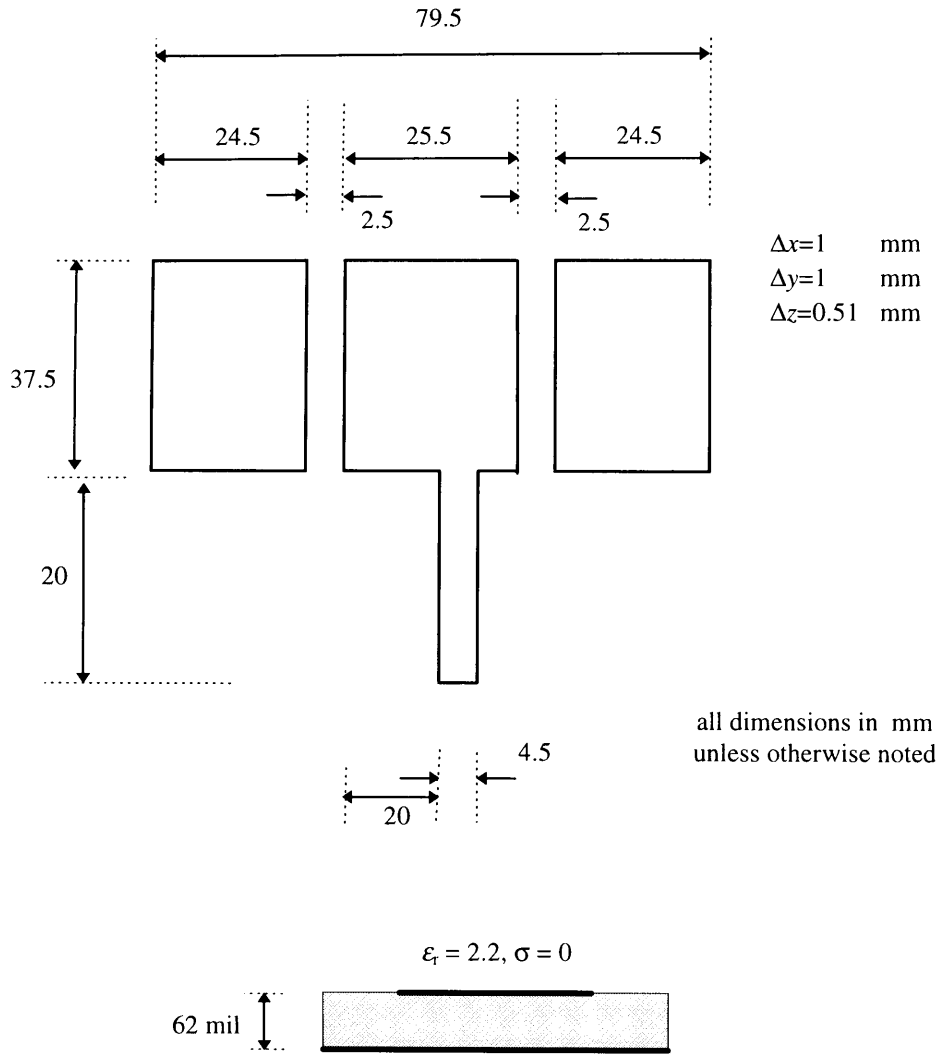

Fig. 5.1 The three-patch microstrip coplanar parasitic antenna array structure [15].

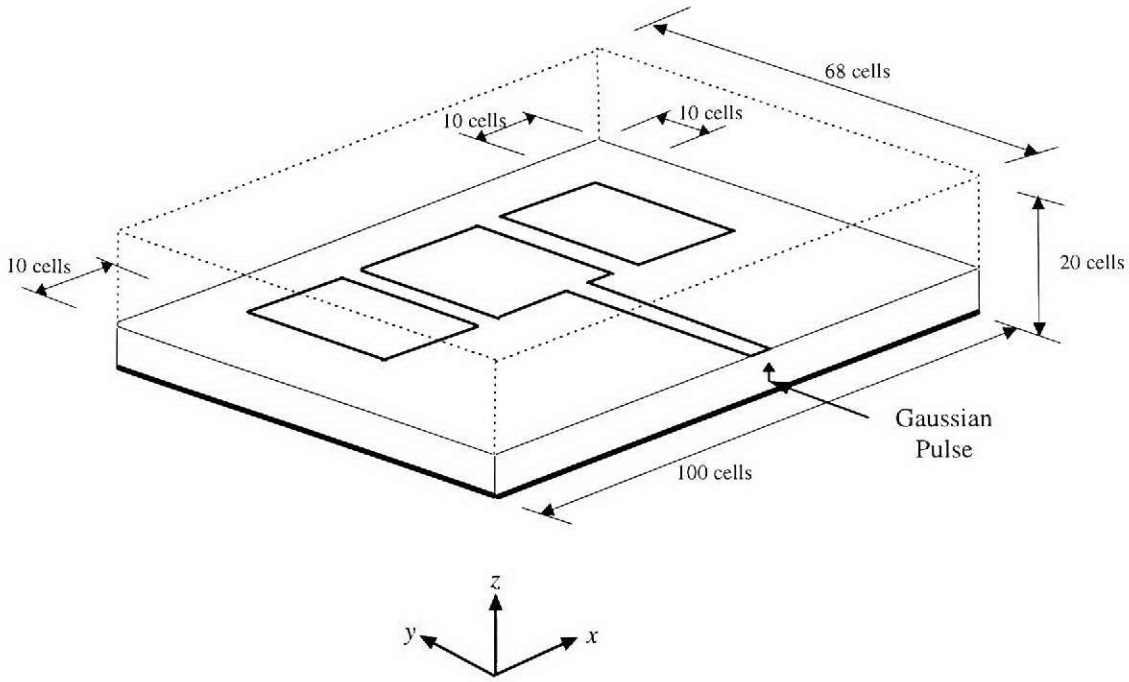

Fig. 5.2 3D diagram of the three-patch coplanar parasitic antenna

5.3 COMPUTED RESULTS

The structure of the model is given in Fig. 5.1 and Fig. 5.2. There are two sets of simulations. The first set is based on the structure put forward by Zimmerman and Lee [15]. For this computation, Δx = 1 mm, Δy = 1 mm and Δz = 0.51 mm. The workspace is $100 \times 68 \times 20$ for a total of 136,000 cells. 10 cells are kept on the left, right and back side of the model for stability of the simulation. The run to determine the total voltage for the return loss used 4000 time steps. In

the region of the patches, the largest grid size is 1 mm. This grid spacing corresponds to 20 cells/wavelength in the dielectric substrate at 10 GHz. The calculated frequency response agreed well with the measurements at this frequency. The primary region of interest is around 4 GHz.

Here a Gaussian pulse of pulse width T = 50 ps and $t_0 = 3 \times T$ is used (see equation 1.2 and Fig. 1.2 and Fig. 1.3). The Gaussian pulse is truncated at 300 ps when the pulse has fully launched. Keeping in mind the Courant stability condition (2.8), the *magical time step* Δt is equal to 1.3797 ps. Magical time step, is the value of Δt which is exactly equal to the courant stability value from (2.8). For a practical approach, Δt taken for this simulation is 75 % of the calculated value, which is equal to 1.0348 ps.

During the modeling of the structure, dimensions in decimal points are observed. This is impossible to represent in a structure as one cannot have a half cell. The actual dimensions of the three patches are 24.5 mm, 25.5 mm and 24.5 mm respectively from left to right. Due to the decimal points in the modeling, numbers are rounded off to the nearest integer. This leads to approximation of patch model, rather than actual representation.

To eliminate this inaccuracy, a finer cell dimension is chosen. In the second set, the dimensions are Δx = .5 mm, Δy = .5 mm and Δz = 0.51 mm. As the cell size decreases, the total number of cells increases. Here the workspace is

$180 \times 126 \times 20$ for a total of 453,600 cells, nearly three and a half times more cells than for set I. Like for set I, 10 cells are kept on the left, right and back side of the model for stability of the simulation. The run to determine the total voltage for the return loss used 3000 time steps. In the region of the patches, the largest grid size is .51 mm. Here, the time step Δt is 0.8 ps.

The frequency dependent scattering matrix coefficient is given by

$$[V]^{ref} = [S]\,[V]^{inc} \tag{5.2}$$

where $[V]^{ref}$ and $[V]^{inc}$ are the reflected and incident voltage vectors, respectively, and $[S]$ is the scattering matrix. To accomplish this, the vertical electric field underneath the center of each microstrip port is recorded at every time step. The field value is assumed to be proportional to the voltage (which could be easily obtained by numerically integrating the vertical electrical field) when considering the propagation of the fundamental mode. To obtain the scattering parameter $S_{11}(\omega)$, the incident and reflected waveforms must be known. The FDTD simulation calculates the sum of incident and reflected waveforms. To obtain the incident waveform, the calculation is performed using only the feed line, which will now be of infinite extent (i.e., from source to far absorbing wall). This incident waveform may now be subtracted from the incident plus reflected waveform to yield the reflected waveform for the parasitic array. The scattering

parameters, S_{11}, may then be obtained by simple Fourier transform of these transient waveforms as

$$S_{11}(\omega) = \frac{\text{FFT}\ \{V_1^{\text{ref}}(t)\}}{\text{FFT}\ \{V_1^{\text{inc}}(t)\}} \tag{5.3}$$

Note that the reference plane are chosen with enough distance from the circuit discontinuities to eliminate evanescent waves [12].

5.4 VALIDATION

The main goal is to analyze the scattering parameter S_{11} given by equation (5.3). The measured center frequency, according to Zimmerman and Lee [15], is 3.84 GHz. From the two sets of simulated and the simulation result of Zimmerman and Lee [15],a comparative table is given below.

Measured Center Frequency [15] = **3.84** GHz

	Center Frequency	Error %
Set I [Author]	3.66 GHz	4.7 %
Set II [Author]	3.8 GHz	1.05 %
Zimmerman & Lee [15]	3.91 GHz	1.8 %

Fig. 5.3 Comparison study of center frequency for the three-patch microstrip coplanar parasitic antenna array.

Zimmerman and Lee [15] computed the minimum S_{11} of -26 dB against the experimental value of -41 dB. In this simulation, for set I, the drop is -37 dB while for set II, it is -48 dB.

	Drop in S_{11}
Experimental [15]	-41 dB
Set I [Author]	-37 dB
Set II [Author]	-48 dB
Zimmerman & Lee [15]	-26 dB

Fig. 5.4 Comparison study of drop in S_{11} at the center frequency for the three-patch microstrip coplanar parasitic antenna array.

From the graphs, it can be seen that, in my simulation for set I, the drop around 3.6 GHz, is deep but appears before 3.84 GHz, as observed from the experimental results [15]. The first drop around 2.6 GHz is very deep compared to the experimental result. Also it can be seen that the plot is not smooth. It looks quiet curvy. This is due to the Absorbing Boundary Condition used, which is the

first order Mur's ABC. This could also have been caused by the approximation of the model with decimal points in the picture.

In the second set, a much smoother curve is observed. The drop in S_{11} is very very close to the experimental drop. But the first small drop, around 2.6 GHz is not observed here at all. And S_{11} at 2.5 GHz is higher than the experimental result [15]. In this set, a much finer cell size is used, which could have contributed to a smother curve. In fact the cell sizes in the x-axis and the y-axis are half the size used for set I. This leads to nearly twice as much cells in the x and the y direction. As the building block size gets bigger, more time is needed to analyze the complete structure.

It is seen that as the cell size becomes smaller, it increases the number of cells required in the structure. This results in increase of computational cost. For both sets of simulation, the results are close to the experimental result of [15]. For both the simulations, the first order Mur's Absorbing Boundary Condition is used. Better result could have been observed, if a better ABC had been used, for example the second order Mur's ABC.

S_{11} parameter for three-patch microstrip coplanar antenna array (case III-set I)

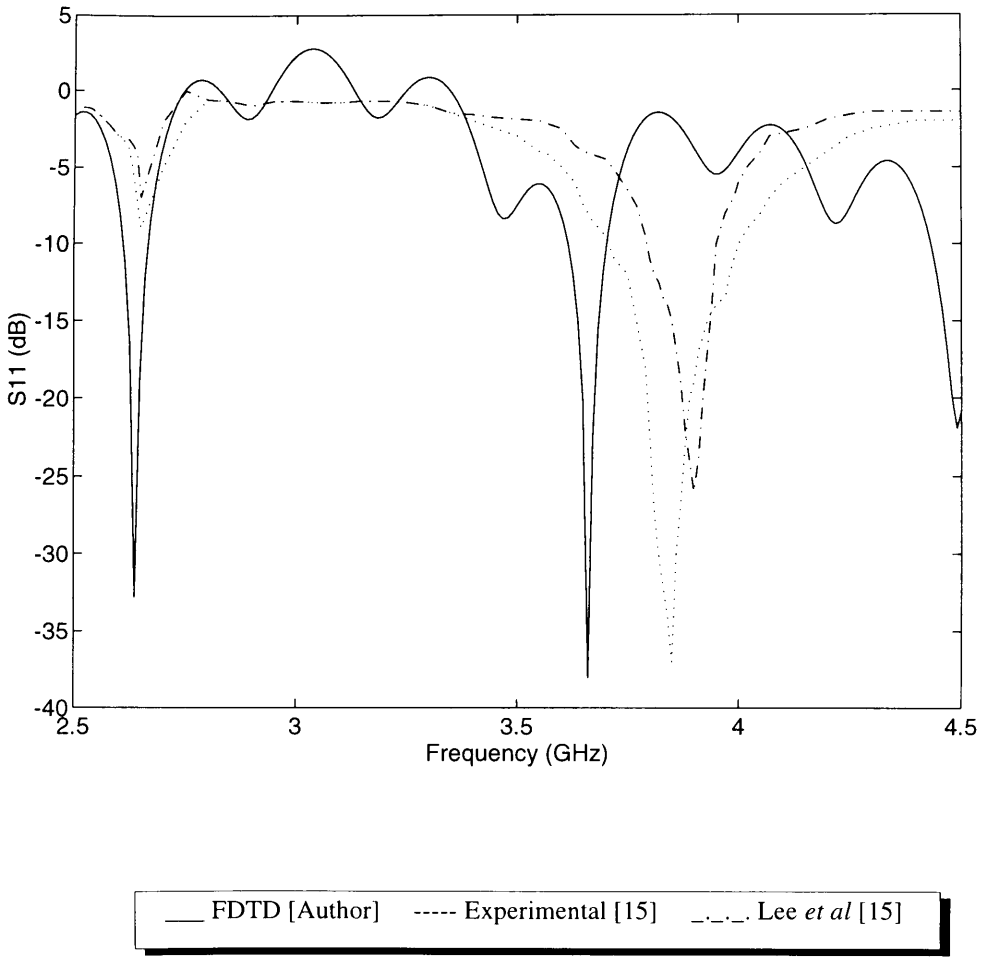

Fig. 5.5 S_{11} parameter for a three-patch microstrip coplanar parasitic antenna array with , Δx = 1 mm, Δy = 1 mm and Δz = 0.51 mm. The center frequency, based on experimental results [15] is around 3.84 GHz.

S_{11} parameter for three-patch microstrip coplanar antenna array (case III- set II)

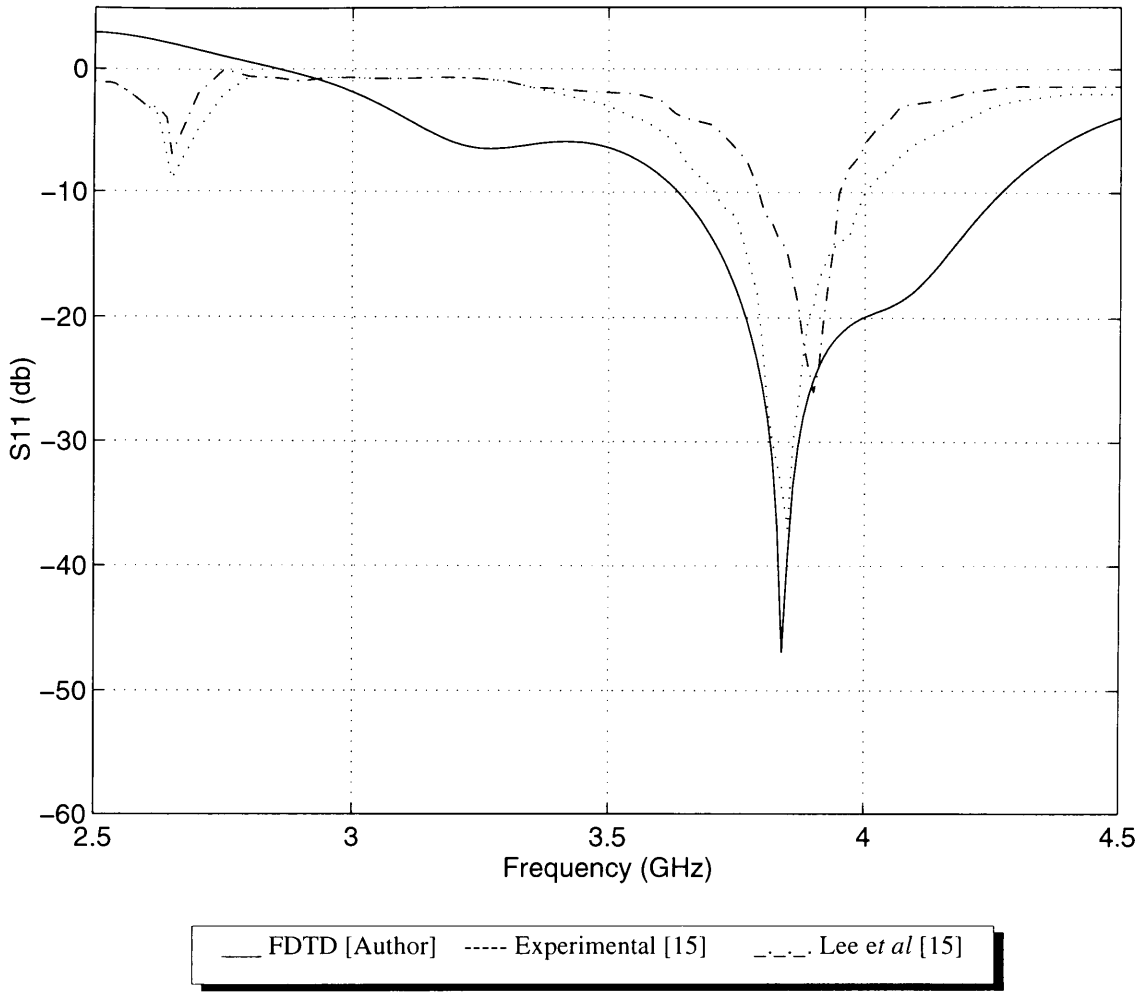

Fig. 5.6 S_{11} parameter for a three-patch microstrip coplanar parasitic antenna array with , Δx = 0.5 mm, Δy = 0.5 mm and Δz = 0.51 mm. The center frequency, based on experimental results [15] is around 3.84 GHz.

Chapter 6

Conclusion and Future Works

CONCLUSION

In this thesis research work, FDTD method is used to analyze multi-conductor transmission line (MTL) and three-patch microstrip coplanar parasitic antenna array. Under MTL, two different models are analyzed. The first model (case I) is a simple two-conductor MTL based on Kraus [8]. Kraus put forward an analytical method (using BASIC program) for the analysis of transmissin line. Here, the FDTD method is used to analyze the structure and the results are compared to Kraus [8]. Furthermore the same model is simulated using the SPICE software. Good results are observed for all the three methods of simulations. As can be seen in Fig. 4.9 and Fig. 4.10, the simulations are very much in agreement with each other. As a pre-requirement for FDTD analysis, the per-unit-length inductance L and capacitance C is determined first. These values depend on the radius of the conductors and the distance between them (center to center). Here, the MTL models are simulated as ribbon cables. Simulation of uniform parallel lines such as ribbon cable has been studied by Shengyao Hu [24]. He has applied FDTD algorithm for analysis of different ribbon cable models.

The second model (case II) is a three-conductor MTL. The FDTD method is used to analyze the Near-End voltage of the transmission line. For validation of this simulation, the three-conductor MTL model is represented with two-wires lines as put forward by Marx *et al* [5]. A proof of this equivalency is also presented in chapter 4.2.2.1. It is then simulated using SPICE software. For the three-wire model, different cell sizes and time steps combinations are presented. There are a total of three different combinations for case II. The first one has NDZ=4 and NDT=60. Likely, the second one has NDZ=6 and NDT=60 and the last one has NDZ=6 and NDT=100. From Fig. 4.16, it can be seen that the combination of NDZ=6 and NDT= 100 has the best result with respect to the SPICE simulation.

For the two-conductor and three-conductor MTL models, a two-dimensional, 2D, FDTD code written in FORTRAN is used. Apart from the main code, two other FORTRAN programs are also used to calculate the per-unit-length parameters of the models which are used as a part of the input data for the main FDTD code. For these MTL models, the two-dimensional FDTD code does not require any ABC, as the models have a source and load resistance.

The third model is a three-patch microstrip coplanar parasitic antenna array. While the first two models are based on Paul [6], the three-dimensional FDTD code is based on Kunz [3]. The numerical results of scattering parameter are validated with the experimental result obtained from [15] and the results of

Zimmerman and Lee [15]. For this model, there are two different simulations. The first simulation uses the cell size described by Lee *et al* [15]. The only drawback with these cell sizes is, the patch size results in fraction of a cell, which is not possible in the FDTD algorithm. For example, the 24.5 mm wide patch needs exactly twenty four and a half cells. There cannot be a half cell. Due to this, the number is rounded off to the nearest integer. This results in inaccurate model representation which leads to inaccurate simulation. In the second simulation, a smaller cell size is chosen in such a way that fractional cells are not encountered. Though this leads to larger number of cells, the model representation is better leading to more accurate simulation. From Fig. 5.5 and 5.6, it can be seen that the second set of simulation is more closer to the experimental result. The first set of simulation has very unstable curves. In both the cases, the Mur's first order ABC is used. The second order ABC is more accurate, but is computer costly. There are different types of ABC that can be used, but in this thesis research work, only the Mur's first order ABC is used.

One of the most important and difficult task in FDTD simulation is to choose the correct size of grid cell and then the time step. The Courant stabiltiy condition is given by the equation (2.8) for a three dimenasional FDTD algorithm and equation (4.7) for a two-dimensional FDTD algorithm. The time step is usually chosen less than the calculated time step [6], given by equation (2.8) and

equation (4.6). In general, it is about 70-80% of the calculatd Δt. In this thesis work, the time step Δt is around 80% of the calculated time step.

For all the three models, the FDTD simulation were very close to the experimental result or results using some other method, like SPICE and BASIC program. It is clearly seen that FDTD is an efficient and accurate tool to model and analyze multi-conductor transmission line as well as different microstrip antennas and arrays. The popularity of FDTD method in the recent years also indicate that this method has been accepted in the industry.

FUTURE WORKS

For future works, different microstrip patch antenna or array can be considered. Provided a better and larger computing environment, smaller grid cells can be considered and larger models can be simulated. For the stability of the system, a higher order absorbing boundary condition can be considered. These high order ABC's are usually complex and need more memory for computation.

References

[1] K. S. Yee, "Numerical solution of initial boundary value problems involving Maxwell's equations in isotropic media", *IEEE Transactions on Antennas and Propagation*, vol. AP-14, May 1966, pp. 302-307.

[2] G. Mur, "Absorbing boundary conditions for the finite-difference approximation of the time-domain electromagnetic-field equations," *IEEE Transactions on Electromagnetic Compatibility*, vol. EMC-23, No. 4, November 1981, pp. 377-382.

[3] K. S. Kunz and R. J. Luebbers, *The Finite-Difference Time Domain Method in Electromagnetics*, CRC Press Inc., Florida, 1993.

[4] R. J. Luebbers, K. S. Kunz, M. Schneider and F. Hunsberger, "A finite-difference time-domain near zone to far zone transformation," *IEEE Transactions on Antennas and Propagation*, vol. 39, No. 4, April 1991, pp. 429-433.

[5] K. D. Marx and R. I. Eastin, "A configuration-oriented SPICE model for multi-conductor transmission lines with homogeneous dielectrics," *IEEE Transactions on Microwave Theory and Techniques*, vol. MTT-38, August 1990, pp. 1123-1129.

[6] C. R. Paul, *Analysis of Multi-conductor Transmission Lines*, John Wiley & Sons Inc., NY, 1994.

[7] A. Taflove, *Computational Electrodynamics: The Finite-Difference Time-Domain Method*, Norwood, MA, Artech House, 1995.

[8] J. D. Kraus, *Electromagnetics*, Fourth Edition, McGraw-Hill Inc., NY, 1992.

[9] D. K. Cheng, *Field and Wave Electormagnetics*, Second Edition, Addison-Wesley Publishing Company, NY, 1989.

[10] R. L. Burden, J. Douglas Faires, *Numerical Analysis*, Fifth Edition, PWS Publishing Company, Boston, 1993.

[11] J. Keown, *PSpice and Circuit Analysis*, Second Edition, Macmillan Publishing Company, NY, 1993.

[12] D. M. Sheen, S. M. Ali, M. D. Abouzahra and J. A. Kong, "Application of the three-dimensional finite-difference time-domain method to the analysis of planar microstrip circuits," *IEEE Transactions on Microwave Theory and Techniques*, vol. 38, No. 7, July 1990, pp. 849-857.

[13] L. W. Couch II, *Digital and Analog Communication Systems*, 4th edition, Macmillan Publishing Company, NY, 1993.

[14] W. D. Becker, S. Chebolu and R. Mittra, "Finite Difference Time Domain modeling of high speed electronic packages," *Microwave Journal*, December 1995, pp. 62-74.

[15] M. L. Zimmerman and R. Q. Lee, "Use of the FDTD method in the design of microstrip antenna arrays," *International Journal of Microwave and Millimeter-Wave Computer-Aided Engineering*, Vol. 4, No. 1, 1994, pp. 58-66.

[16] C. R. Paul, "Incorporation of Terminal Constraints in the FDTD Analysis of Transmission Lines," *IEEE Transactions on Electromagnetic Compatibility*, Vol. 36, No. 2, May 1994, pp. 85 - 91.

[17] X. Zhang and K. K. Mei, "Time-Domain Finite Difference Approach to Calculation of the Frequency-Dependent Characteristics of Microstrip Discontinuities," *IEEE Transactions on Microwave Theory and Techniques*, vol. 36, No. 12, December 1988, pp.1775-1787.

[18] R. J. Luebbers, K. S. Kunz and K. A. Chamberlin, "An Interactive Demonstration of Electromagnetic Wave Propagation Using Time-Domain Finite Differences," *IEEE Transactions on Education*, Vol. 33, No. 1, February 1990, pp.60-68.

[19] K. Naishadham and X. P. Lin, "Minimization of Reflection Error Caused by Absorbing Boundary Condition in the FDTD Simulation of Planar Transmission Lines," *IEEE Transactions on Microwave Theory and Techniques*, vol. 44, No. 1, January 1996, pp.41-46.

[20] R. E. Zeimer and W. H. Tranter, *Principles of Communications - Systems, Modulationa and Noise*, Third Edition, Houghton Mifflin Company, Boston, 1990

[21] *Matlab Reference Guide*, The MathWorks, Inc., Natick MA, August 1992

[22] C. M. Furse and O. P. Grandhi, " Why the DFT is Faster Than the FFT for FDTD Time-to-Frequency Domain Conversions", *IEEE Microwave and Guided Wave Letters*, vol. 5, no. 10, 1995, pp. 326-328.

[23] Peter G. Petropoulos, " Stability and Phase Error Analysis of FD-TD in Dispersive Dielectrics, " *IEEE Trans. on Antennas and Propagation*, vol. 42, no. 1, 1994, pp. 62-69.

[24] Shengyao Hu, *Analysis of Uniform Parallel Transmission Line and Microstrip Branch Line Coupler using Finite-Difference Time-Domain Method*, Master's Thesis, Electrical and Computer Engineering Department, Florida International University, August, 1996.

[25] James C. Rautio, " Experimental Validation of Electromagnetic Software, " *International Journal of Microwave and Millimeter-Wave Computer-Aided Engineering*, vol. 1, no. 4, 1991, pp. 379-385.

Appendix

SPICE CODE for Analysis of two-conductor MTL

```
SPICE MTL MODEL RIBBON two-conductor, risetime = 15 ns
VS    7     0     PULSE(0 10 0 15N 15N 100N 1600N)
RS    7     1     20
RL    2     0     200
V1    1     3
V2    2     4
EC1   3     0     POLY( 1)(5,0) 0 1
FC1   0     5     POLY( 1) V1 0 1
EC2   4     0     POLY( 1)(6,0) 0 1
FC2   0     6     POLY( 1) V2 0 1
T1    5     0     6     0     Z0=9.993076E+01      TD=3.335639E-07
.TRAN       1N    1600N       0     1N
.PRINT      TRAN V(5) V(6)
.PLOT       TRAN V(5) V(6)
.PROBE
.END
*SUBCIRCUIT MODEL OF A MULTI-CONDUCTOR TRANSMISSION LINE*
*       NUMBER OF CONDUCTORS=  1
*       TOTAL LINE LENGTH (METERS)= 1.00000E+02
*       L(  1,  1)= 3.33333E-07
*       C(  1,  1)= 3.33795E-11
.SUBCKT MTL
+1
+2
V1    1     3
V2    2     4
EC1   3     0     POLY( 1)(5,0) 0 1
FC1   0     5     POLY( 1) V1 0 1
EC2   4     0     POLY( 1)(6,0) 0 1
FC2   0     6     POLY( 1) V2 0 1
T1    5     0     6     0     Z0=9.993076E+01      TD=3.335639E-07
.ENDS MTL
```

Table 1.1 SPICE program to simulate two-conductor transmission line with rise and fall time of 15 ns and pulse width of 100 ns. The final solution time is 1600 ns. $R_S = 20\ \Omega$, $R_L = 200\ \Omega$ and $R_O = 100\ \Omega$. The magnitude of the pulse is 10 V.

SPICE CODE for Analysis of three-conductor MTL

```
* MTL Model Using Two-Wire Delay Lines
*
.OP
VS    1 0 PULSE(0 1 0 12.5N 12.5N 7.5N 200N)   ;Source
RS    1 2 50                                    ;Source
RL    9 0 50                                    ;Load
RNE  10 0 50                                    ;Near End
RFE  17 0 50                                    ;Far End
*
T10   2   0   9   0 Z0=323.6 TD=15.56N ;Transmission Line
T12 2   17   9 10 Z0=1522   TD=15.56N ;Coupled & Transmission
T20 17   0 10   0 Z0=323.6 TD=15.56N ;Transmission Line
*
.TRAN 0.5N 200N                        ;Time Domain Analysis
.OPTIONS LIMPTS=801 PIVTOL=1.0E-16
.PRINT TRAN V(1) V(2) V(9) V(17) V(10)
.lib nom.lib
.probe
.END
```

Table 1.2 SPICE program to simulate three-conductor transmission line with rise and fall time of 12.5 ns and pulse width of 7.5 ns. The final solution time is 200 ns. R_S = 50 Ω, R_L = 50 Ω, R_{NE}=50 Ω and R_{FE}=50 Ω. The magnitude of the pulse is 1V. The characteristic impedance of the two-wire line are z_{o10} = z_{o20} = 323.6 Ω and z_{o12}=1522 Ω. The time delay for the model is 15.56 ns.